Title
SKN-1 is a metabolic surveillance factor that surveils amino acid catabolism pathways to control stress resistance

Author
Frankino, Phillip Andrew

Publication Date
2022

Peer reviewed|Thesis/dissertation

SKN-1 is a metabolic surveillance factor that surveils amino acid catabolism pathways to control stress resistance

By

Phillip Andrew Frankino

A dissertation submitted in partial fulfillment of the

requirements for the degree of

Doctor of Philosophy

in

Molecular and Cell Biology

in the

Graduate Division

of the

University of California, Berkeley

Committee in charge:

Professor Andrew Dillin, Chair

Professor Robert Tjian

Professor Barbara Meyer

Professor Anders Näär

Spring 2022

Abstract

SKN-1 is a metabolic surveillance factor that surveils amino acid catabolism pathways to control stress resistance

By

Phillip A. Frankino

The deleterious potential to generate oxidative stress and damage is a fundamental challenge to metabolism. The oxidative stress response transcription factor, SKN-1/NRF2, can sense and respond to changes in metabolic state, although the mechanism and physiological consequences of this remain unknown. To explore this connection, we performed a genetic screen in *C. elegans* targeting amino acid catabolism and identified multiple metabolic pathways as regulators of SKN-1 activity. We found that genetic perturbation of the conserved amidohydrolase *T12A2.1/amdh-1* activates a unique subset of SKN-1 regulated detoxification genes. Interestingly, this transcriptional program is independent of canonical P38-MAPK signaling components but requires the GATA transcription factor ELT-3, nuclear hormone receptor NHR-49, and mediator complex subunit MDT-15. This activation of SKN-1 is dependent on upstream histidine catabolism genes HALY-1 and Y51H4A.7/UROC-1 and may occur through accumulation of a catabolite, 4-imidazolone-5-propanoate (IP). Triggering SKN-1 activation results in a physiological trade off of increased oxidative stress resistance but decreased survival to heat stress. Together, our data suggest that SKN-1 is a key surveillance factor which senses and responds to metabolic perturbations to influence physiology and stress resistance.

Table of Contents

Acknowledgements

I find it difficult to express my gratitude for the countless people who deserve credit for helping me accomplish what I have in these last six years. There are too many to thank for the words of encouragement, much needed drinks and general comradery throughout my time at Berkeley. I think first and foremost, I must thank my rock, my everything, my all - Samira. Your endless support and encouragement is the single most important factor in my success. On days I was down, you picked me up. On days I was up, you pushed me higher. Our life together is just starting but I will never forget the persistence and sacrifices you gave to keep us where we needed to be. Thank you for that, I love you bean.

Next, I need to thank my family. To my mother and father, Jennifer and Tony, who always tried to do their best in raising me. You showed me that anything is possible and that I can accomplish anything I set my mind to. It was not easy to adjust from a tiny town of less than 7,000 people to the bay area of over 7 million, but the values instilled in me at that house on Revere drive will forever motivate me and keep me on the right track. Thank you for supporting my decision to chase my dreams on the west coast and offering encouragement wherever you could. It hasn't been easy being so far away from you, but I know you have only been a call away. To my brothers Chris and Anthony and to my sister, Allison. You inspire me to keep pushing through. I will always have best friends in my siblings who I can call, day or night, from all the way across the country.

To my lab mates and friends who have helped me along the way - what a funky bunch you all are. I will never be able to express to you what your friendship has meant to me over the years, but you have all been as integral to my success as anyone I could acknowledge. I enjoyed the casual lab conversations we had over whiskey and beer. I will always remember the late nights at Triple Rock or Eureka, which turned to late late nights at Spats. I won't ever forget the ski trips taken when we needed to disappear for the weekend. Those times were essential to maintaining my sanity and as important to my success in graduate school as pretty much anything else. I know I have lifelong friends in every one of you, and for that I am grateful.

To Andy - thank you for your patience and space to grow as a scientist and person. Although there were times that I felt like I lost the road ahead, you were always there to let me know that it wasn't that far off. Thanks to my thesis committee members Professor Robert Tjian, Professor Barbara Meyer and Professor Anders Naar for helpful comments and advice on my thesis work and for believing in me along the way.

Chapter I: Introduction

Metabolism and metabolic products as signaling molecules

Metabolism is central to normal cell function and is dysregulated in human diseases such as metabolic syndrome, diabetes, and cancer (DeBerardinis and Thompson, 2012). In the most basic sense, metabolism is the sum of all biochemical reactions in the cell including reactions that create or break down complex molecules (anabolism and catabolism, respectively). The catabolism of amino acids leads to the accumulation of breakdown products, or catabolites, essential for creating cellular energy through the tricarboxylic acid (TCA) cycle and cellular respiration (Akram, 2014; Martínez-Reyes and Chandel, 2020). All 20 proteinogenic amino acids can be broken down to form one, or multiple, of the important intermediate metabolites that flux through the TCA cycle: alpha-ketoglutarate, succinyl-CoA, fumarate, oxaloacetate, pyruvate, acetyl-CoA and acetoacetyl-CoA. Amino acids are classified as either glucogenic or ketogenic depending on the intermediates formed by their catabolic pathways. Glucogenic amino acids are those that, when broken down, lead to catabolites that can be used for the synthesis of glucose via gluconeogenesis such as alpha-ketoglutarate, succinyl-CoA, fumarate, oxaloacetate and pyruvate. Ketogenic amino acids are those that form acetyl-CoA or acetoacetyl-CoA, metabolites crucial for the formation of ketone bodies. Some amino acids can be both glucogenic and ketogenic, leading to multiple metabolites that can feed into either pathway.

Outside of their role in creating cellular energy, catabolites have also been identified as signaling molecules that affect both normal cell function and disease. For example, tryptophan catabolites are known immunomodulators, and elevated expression of tryptophan catabolism enzymes is associated with cancer progression and poor prognosis (McGaha et al., 2012). Additionally, the histidine catabolite, imidazolone propionate, is elevated in type 2 diabetic patients and has been shown to impair insulin signaling (Chong et al., 2018; Molinaro et al., 2020). Intriguingly, catabolic enzymes are often cell type and tissue specific, leading to important catabolite buildup that dictates intracellular signaling or cellular stress resistance. An interesting example of this comes from the discovery that urocanate buildup in the epidermis may act as a natural sunscreen, protecting against UV induced damage (Tabachnick, 1957; Ženíšek et al., 1955). Notably, animals express the first enzyme in the histidine catabolism pathway, histidase, but lack the subsequent enzyme, urocanase, in the epidermis leading to the buildup of this protective molecule in the skin (Bender, 2012). Apart from their signaling and protective roles, amino acid catabolites can also cause damage. Accumulation of the lysine catabolite, saccharopine, causes mitochondrial dysfunction in mice and worms (Zhou et al., 2018). Many inborn errors of metabolism (IEMs) are caused by metabolite buildup, damage and disease. Humans with mutations in 4 of the 5 tyrosine catabolism enzymes can cause IEMs, including Type 1 tyrosinemia (Morrow and Tanguay, 2017). Despite their importance, our understanding of the identity, mechanism and physiological consequences of catabolite signaling is incomplete.

The Oxidative Stress Response and SKN-1/NRF2

A key challenge for metabolism is the resolution of deleterious byproducts that can damage cellular components. For example, the electron transport chain of the mitochondria is the main site of ATP generation but also produces harmful reactive oxygen species (ROS), a form of

oxidative stress that damages DNA, lipid membranes and proteins (Nolfi-Donegan et al., 2020). To resolve oxidative damage, cells have evolved a conserved stress response controlled by the transcription factor NF-E2 related factor 2 (NRF2) which upregulates antioxidant synthesis and detoxification enzymes to neutralize oxidants and export toxic molecules from the cell (Blackwell et al., 2015). In humans, NRF2 is in the Cap'n'collar subfamily of the bZIP family of transcription factors which traditionally require a small musculoaponeurotic fibrosarcoma protein (Maf) dimerization partner for stable DNA binding (Ma, 2013). NRF2 transcriptionally upregulates genes helpful for survival and clearance of oxidative stress and damage through the binding of target genes at antioxidant response elements (AREs) in their promoters (Ma, 2013). In *C. elegans*, the functional NRF2 homolog, SKN-1, acts during development, stress response and aging (Sykiotis and Bohmann, 2010). While their modes of DNA binding are slightly different, both SKN-1 and NRF2 function in remarkably similar manners. In *C. elegans,* the oxidative stress response (OxSR) is initiated in response to oxidative stress through a signaling cascade that converges on the conserved MAP kinase (MAPK) pathway, resulting in the phosphorylation and activation of the MAPKK and P38/MAPK homologs (SEK-1 and PMK-1, respectively) (Inoue et al., 2005). Once this signaling cascade is initiated, nuclear factors such as ELT-3, NHR-49, and MDT-15 are required for upregulation of stress response targets (Goh et al., 2014, 2018; Hu et al., 2017; Wu et al., 2016). Together, the OxSR alleviates oxidative stress and restores homeostasis to promote cell and organismal survival.

SKN-1 activity in *C. elegans* is tightly regulated by the E3 ubiquitin ligase adapter protein WDR-23 and cullin4 homolog, DDB-1, which degrade this transcription factor in the absence of stress (Choe et al., 2009). Intriguingly, the exact mechanism of how WDR-23 senses oxidative or xenobiotic stress remains elusive. In mammals, KEAP1 functions in a similar manner to WDR-23, although the mechanism is more established. During oxidative stress, redox sensitive Cysteine residues in KEAP1 are oxidized, breaking its interaction with NRF2 and activating downstream signaling (Sekhar et al., 2010). In *C. elegans*, this negative regulation of SKN-1 is conserved through WDR-23, although WDR-23 is not a sequence homolog of KEAP1. Furthermore, the WDR-23 homolog in humans has also been shown to negatively regulate NRF2, independent of KEAP1, suggesting that the regulation of the OxSR by both of these mechanisms is conserved (Lo et al., 2017). In sum, the regulation of SKN-1/NRF2 is complex and interesting, likely due to the importance of this pathway for organismal resilience and survival over time.

Emerging functions of SKN-1/NRF in metabolism

Historically, SKN-1 is known as the master regulator of the OxSR but emerging literature has implicated it as a metabolic surveillance factor. For example, exogenous supplementation of amino acids are sensed and activate SKN-1-mediated transcription (Edwards et al., 2015). SKN-1 can also respond to changes in proline catabolism to mobilize lipids during starvation (Pang et al., 2014). Furthermore, genetic perturbation of multiple amino acid catabolism pathways activate SKN-1-mediated transcription (Fisher et al., 2008; Ravichandran et al., 2018; Tang and Pang, 2016). Intriguingly, these instances of SKN-1 activation may involve diverse catabolites, integrating the state of multiple metabolic pathways to sense and respond to metabolic imbalance through a single effector. To date, no study has comprehensively probed metabolic pathways to understand the surveillance and response role of SKN-1 in metabolism.

Here, we identify multiple pathways of amino acid catabolism that, when perturbed, activate a distinct transcriptional response driven by SKN-1. Using a mutant of histidine catabolism as a model, we show that this response is independent of canonical MAPK signaling pathways and may partially depend on GCN2 and mTOR homologs *gcn-2* and *let-363*. We also demonstrate the necessity of nuclear factors previously implicated in the OxSR for SKN-1 activation. Interestingly, this response is dependent on the upstream enzymes of the histidine catabolism pathway, suggesting endogenous catabolites may activate SKN-1. Activation of SKN-1 via mutation of the histidine catabolism pathway results in increased oxidative stress resistance at the cost of decreased resistance to heat stress, indicating that SKN-1 mediates a tradeoff between stress response survival. Together, our data uncover a novel metabolic surveillance mechanism driven by SKN-1, which likely works through accumulation of catabolite intermediates, to control susceptibility to stress.

Chapter 2: SKN-1 is a metabolic surveillance factor that affects stress response

Chapter 2.1: Results

To uncover the genetic mechanisms by which SKN-1 serves as a metabolic surveillance factor, we performed an RNAi screen to comprehensively survey amino acid catabolism pathways that, when perturbed, activate a SKN-1 dependent transcriptional response. We constructed a sub-library containing 78 RNAi clones targeting catabolic pathways for all of the 20 proteinogenic amino acids including genes involved in glutathione (GSH) synthesis (Table 1). Using this RNAi sub-library, we assessed SKN-1 activity by measuring the fluorescence of animals expressing GFP downstream of the *gst-4* promoter (*gst-4p::GFP*), a well established reporter of SKN-1 (Link and Johnson, 2002). Notably, we found that knockdown of glutathione synthesis, tyrosine or valine catabolism enzymes activate the SKN-1 reporter as previously described, confirming the ability of our screen to identify known regulating enzymes of, and pathways surveilled by, SKN-1 (Figure 1a, Table 1) (Fisher et al., 2008; Wang et al., 2010). Interestingly, we found that genetic perturbation of histidine, glycine and phenylalanine catabolism led to activation of the SKN-1 reporter gene (Figure 1a, Table 1). Together, these results suggest that SKN-1 is a metabolic regulator which responds to changes in multiple amino acid catabolism pathways, and possibly directly to amino acid levels.

Knockout of histidine catabolism enzyme AMDH-1 triggers a SKN-1-mediated detoxification response

Our screen revealed that the phenylalanine, glycine and histidine catabolism pathways are surveilled by SKN-1, and activate this transcription factor when perturbed. Both phenylalanine, through the phenylalanine hydroxylase *pah-1*, and glycine catabolism, through the glycine cleavage protein *gldc-1*, have established connections to SKN-1 via the NADPH oxidase *bli-3* and antioxidant synthesis, respectively (Calvo et al., 2008). We chose the conserved histidine catabolism pathway as a model to further elucidate this mechanism of SKN-1 activation, as histidine is an essential amino acid and its metabolic pathway remains largely uncharacterized in *C. elegans*. *T12A2.1*, which was renamed **AM**i**D**o**H**ydrolase domain containing protein **1** (*amdh-1)*, is a conserved amidohydrolase in the histidine catabolism pathway that processes its substrate, 4-imidazolone-5-propanoate (IP), to create N-formimino-L-glutamate (FIGLU) (Figure 1b). To further explore the mechanism of SKN-1 surveillance of amino acid catabolic processes, we used CRISPR-Cas9 to generate a putative null allele, *amdh-1*(*uth29),* by introducing a premature stop codon in exon 1 of its coding sequence (Supplement Figure 1). We found that *amdh-1* mutants robustly induce the SKN-1 reporter strain in a SKN-1-dependent manner, compared to wild-type animals (Figure 1c,d). To determine whether *amdh-1* mutation altered global SKN-1 transcription, we analyzed gene expression changes in *amdh-1* mutants versus wild-type animals (Figure 1e,). We found that a unique subset of SKN-1 targets, the detoxification enzyme family of glutathione-s-transferases (GSTs), were among the most upregulated genes in our dataset, suggesting that changing AMDH-1 levels triggers a specific transcriptional output, likely driven by SKN-1. Direct comparison of differentially expressed genes (DEGs) in our dataset to previously published datasets revealed that genes upregulated in *amdh-1* mutants were also highly upregulated in *skn-1(lax188)* gain-of-function animals and downregulated in worms treated with *skn-1* RNAi (Figure 1f) (Nhan et al., 2019; Steinbaugh et

al., 2015). In contrast, downregulated genes in *amdh-1* mutant animals were not differentially regulated under *skn-1* loss or gain-of-function, suggesting that AMDH-1 may also impact SKN-1-independent processes. Interestingly, knockdown of *amdh-1* did not affect the expression of another well-characterized SKN-1 reporter (*gcs-1p::GFP*), further suggesting that there are distinct transcriptional responses modulated by SKN-1 (Supplement Figure 1b,c). Taken together, our data show that perturbation of histidine catabolism upregulates a specific transcriptional program driven by SKN-1, that is only a subset of the general oxidative stress response and is likely tailored for the perturbation of histidine catabolism. This response includes detoxification enzymes but not other known SKN-1 targets such as antioxidant synthesis enzymes.

SKN-1 activation in *amdh-1* mutants is dependent on known oxidative stress regulators but not canonical p38/MAPK or nutrient signaling pathways

Amino acids play essential roles in maintaining energy homeostasis, a process controlled by a few key nutrient regulators (Efeyan et al., 2015). Therefore, we hypothesized that perturbation of histidine catabolism, and thus SKN-1 activation, may be tightly regulated by these nutrient sensing pathways. To test this hypothesis, we knocked down orthologs of nutrient regulators mTORC1/2 (*let-363)*, RRAGA *(raga-1*), AMPK (*aak-2)*, FOXO (*daf-16*), TFEB (*hlh-30*) and GCN2 (*gcn-2*) and surveyed SKN-1 activation in *amdh-1* mutants. Strikingly, we observed that none of these regulators were completely required for SKN-1 activation (Supplement Figure 2a,b). Knockdown of *aak-2* had no effect while *daf-16*, *hlh-30* or *raga-1* further increased SKN-1 activation in *amdh-1* mutants. Notably, *gcn-2* or *let-363* knockdown significantly decreased SKN-1 activation in these mutants, although SKN-1 levels remained over 2 fold greater ($\log2(FC) > 1$) in *amdh-1* mutants compared to wild-type animals fed RNAi against these genes (Supplement Figure 2a,b). Interestingly, we observed increased activation of SKN-1 in *raga-1* knockdown conditions, targeting RRAGA/mTORC1, and suppression of activation upon *let-363* knockdown, targeting both mTORC1/mTORC2. These data suggest that activation of SKN-1 in *amdh-1* mutants may depend on GCN2 and mTORC2 while it is independent of other nutrient regulators AMPK, FOXO, TFEB and mTORC1/RRAGA.

In *C. elegans*, SKN-1 can be activated via phosphorylation by the p38/MAPK ortholog, PMK-1, in a signaling cascade that requires the MAPKK, SEK-1 (Inoue et al., 2005). To assess the requirements of these well established regulators on SKN-1 activation, we tested whether animals with mutations in this pathway can still activate SKN-1 upon *amdh-1* knockdown. We observed that *pmk-1(km25)* and *sek-1(km4)* mutants fail to suppress SKN-1 activation and instead exhibit increased activation with *amdh-1* knockdown (Figure 2a,b). These data show that canonical MAPK regulators are not required for SKN-1 activation in the face of metabolic perturbations and may even negatively regulate this response.

To identify genetic pathways required for SKN-1 activation in *amdh-1* mutants, we performed a genetic suppressor screen using EMS mutagenesis on SKN-1 reporter animals in an *amdh-1(uth29)* background. Using a combination of backcrossing and deep sequencing as previously described (Lehrbach et al., 2017), we identified 6 alleles in 4 genes that are required for SKN-1 activation in *amdh-1* mutants (Supplement Figure 2c). Among the mutants identified was a putative DNA binding domain mutant of *skn-1* that is present across all four isoforms

(Supplement Figure 2c). These worms are slow growing, likely due to the requirement for SKN-1 in development (Bowerman et al., 1992). The discovery of this new SKN-1 allele validates the screen and supports the previous finding that this phenotype is dependent on *skn-1* (Figure 1c,d). Among the remaining mutations found in our screen, we identified a novel SKN-1 regulator, *suco-1,* and a previously identified regulator, *elt-3*, as suppressors of SKN-1 activity in *amdh-1(uth29)* mutant animals (Supplement Figure 2c). RNAi knockdown of *suco-1* or *elt-3* suppress SKN-1 activation in *amdh-1* mutants, phenocopying the EMS mutants and suggesting a causal relationship between these regulators and SKN-1 (Figure 2c,d). *suco-1* encodes an ortholog of the SLP/EMP65 complex identified in yeast to function in ER protein homeostasis, a process previously implicated in the OxSR (Glover-Cutter et al., 2013; Zhang et al., 2017). *elt-3* is a required factor for induction of OxSR gene expression (Hu et al., 2017). The existing role of *elt-3* in the OxSR prompted further investigation of other required nuclear factors.

SKN-1 drives expression of detoxification enzymes, such as GST-4, under conditions of oxidative stress with the help of nuclear factors like ELT-3, nuclear hormone receptor NHR-49, and mediator complex subunit, MDT-15 (Goh et al., 2014, 2018; Hu et al., 2017; Wu et al., 2016). As these nuclear factors are well established to be required for both stress response gene transcription and survival upon oxidative stress, we hypothesized that they may also be required for SKN-1 activation in *amdh-1* mutants. We found that knockdown of *nhr-49* or *mdt-15* significantly suppressed the activation of SKN-1 in *amdh-1(uth29)* mutants (Figure 2c,d). Together, these data suggest that activation of SKN-1 in animals with perturbed histidine catabolism is dependent on canonical nuclear regulators of the OxSR.

Enzymes HALY-1 and Y51H4A.7/UROC-1 are required for SKN-1 activation in AMDH-1 mutants

Through the EMS suppressor screen, we also identified 3 independent alleles of *haly-1 (uth92, uth93, uth95)*, the conserved histidine ammonia lyase that is rate limiting for the histidine catabolism pathway, as suppressors of SKN-1 activity (Figure 3a, Supplement Figure 2c). Expression of a wild-type copy of *haly-1* rescued the suppression of SKN-1 activation in *haly-1(uth92)* and *haly-1(uth93)* mutants, confirming the causative nature of these mutations (Supplement Figure 3a,b).

AMDH-1 is the third enzyme in the catabolism of histidine to glutamate. Two upstream enzymes conserved in *C. elegans*, HALY-1 and Y51H4A.7*,* renamed to **UROC**anate hydratase protein 1, UROC-1, catalyze histidine to glutamate conversion through the formation of two intermediate catabolites, urocanate and IP (Figure 1b). One possible mechanism, supported by the finding that *haly-1* mutants suppress SKN-1 activation in *amdh-1* mutants, is that catabolite buildup activates SKN-1. To explore this possibility, we performed epistasis experiments using RNAi to knock down the upstream enzymes of the histidine catabolism pathways in *amdh-1* mutant animals. If a buildup of the second catabolite, IP, leads to SKN-1 activation, knockdown of *uroc-1* would also suppress SKN-1 activation. We found that RNAi knockdown of *haly-1* phenocopies the suppression seen in *haly-1* mutants and that *uroc-1* completely suppressed the activation of SKN-1 in *amdh-1* mutants (Figure 3b,c). These findings support the hypothesis that SKN-1 activation in these mutants proceed through a catabolite intermediate, likely IP.

Histidine supplementation amplifies SKN-1 activation in AMDH-1 mutants

The poor solubility and short half-life of catabolites upstream of *amdh-1*, urocanate and IP, prevented the direct testing of catabolite activation. Rather, we tested whether increasing flux through the histidine catabolism pathway differentially affects *amdh-1* mutants compared to wild-type animals. Notably, this differential activation would depend on one or both upstream enzymes, *haly-1* and *uroc-1*, if the mechanism proceeds through a catabolite intermediate. Accordingly, we supplemented SKN-1 reporter animals, in both wild-type and *amdh-1* mutant backgrounds, with histidine. Strikingly, *amdh-1* mutant animals exhibit a robust activation of SKN-1 upon histidine supplementation when compared to wild-type animals (Figure 3d,e). Indeed, this activation is partially suppressed by knockdown of *haly-1* and completely suppressed by knockdown of *Y51H4A.7/uroc-1* (Figure 3f,g). These data further support a model that the catabolite intermediate IP drives SKN-1 activation.

amdh-1 mutants are sensitive to heat stress and resistant to oxidative stress

SKN-1 can be either beneficial or detrimental to organismal physiology and aging depending on expression level. For example, moderate activation of SKN-1 extends lifespan while high expression can shorten lifespan (Paek et al., 2012; Tullet et al., 2008). Moreover, activation of SKN-1 increases oxidative stress survival while decreasing survival to other stressors such as heat (Crombie et al., 2016; Deng et al., 2020). Considering the strong induction of SKN-1 upon *amdh-1* loss of function, we questioned whether this activation was beneficial or detrimental to organismal health. First, we assessed the lifespans of *amdh-1(uth29)* mutants compared to wild-type animals and found no significant effect on adult lifespan (Figure 4a). We next tested whether SKN-1 activation affects the animal's ability to survive different stress conditions. Predictably, *amdh-1* mutants are resistant to tert-butyl hydroperoxide, an organic peroxide known to induce the OxSR, likely representing a "priming" effect that SKN-1 has on these animals to survive oxidative stress (Figure 4b). Surprisingly, we observed a stark change in resistance to thermal stress, a 50% decrease in thermotolerance compared to wild-type animals. The decreased thermotolerance of *amdh-1* mutants was completely rescued by RNAi knockdown of *skn-1*, suggesting that SKN-1 activation is detrimental to thermotolerance (Figure 4c). Additionally, stress survival on tunicamycin was also modestly reduced (Figure 4d). Notably, we did not observe a change in any other fluorescent reporters that measure the activation of other cellular stress responses (Supplement Figure 4a-e). Together, our data suggest that SKN-1 activation in *amdh-1* mutants drives a physiological tradeoff that preserves survival under oxidative stress conditions at the cost of heat and ER stress resilience without a significant impact on these well defined transcriptional stress responses.

Chapter 2.2: Discussion

SKN-1 as a metabolic surveillance factor

Previous studies have reported that perturbation of tryptophan, threonine, or proline catabolism evoke a SKN-1-mediated transcriptional response (Fisher et al., 2008; Pang et al., 2014; Tang and Pang, 2016; Ravichandran et al., 2018). Our work expands this list to include glycine, valine, phenylalanine and histidine catabolism as surveillance targets of SKN-1, which can have direct effects on stress resilience. Further, we demonstrate that knockdown of a conserved

amidohydrolase in the histidine catabolism pathway leads to a buildup of a catabolite, likely IP, to activate a transcriptional response driven by SKN-1. This response appears partially dependent on nutrient regulators, GCN-2 and mTORC2, and OxSR regulators ELT-3, NHR-49 and MDT-15 (Figure 4e). It is unknown whether SKN-1 activation in this context is a direct or indirect consequence of catabolite buildup, however the activation of SKN-1 results in a clear trade-off of increased oxidative stress resilience for increased sensitivity to heat stress.

While it is unknown whether SKN-1 activation in this context is a direct or indirect consequence of catabolite buildup, existing literature suggests that multiple amino acid catabolites can signal to SKN-1. For example, proline catabolism is modulated upon pathogen exposure to accumulate the intermediate pyrroline-5-carboxylate (P5C) to activate SKN-1 through ROS production (Tang and Pang, 2016). Other reports have demonstrated that disruption of tyrosine catabolism, through mutation in fumarylacetoacetate hydrolase, *fah-1*, causes stunted growth and intestinal degradation through tyrosine catabolites (Fisher et al., 2008). Intriguingly, *fah-1* mutants have increased SKN-1 activity (Fisher et al., 2008). Our findings help unify these previously observed phenomena and suggest that SKN-1 may integrate information from multiple catabolite activators into transcriptional programs to affect physiology.

Interestingly, in response to mutation of *amdh-1*, there is an upregulation of a subset of target genes including *gst-4*, but not another well known SKN-1 target, *gcs-1*. Previous studies have reported such discordance between SKN-1 activation and the expression of these specific genes. For example, in an RNAi screen for genes that activate a *gcs-1* reporter when knocked down, Wang and colleagues found that a small subset of them failed to also activate expression of *gst-4* (Wang et al., 2010). Furthermore, SKN-1 has been shown to upregulate specific subsets of genes depending on the stress encountered, demonstrating that the regulation of SKN-1 is complex and likely represents the ability of this transcription factor to regulate tailored responses subject to the nature of the perturbation (Oliveira et al., 2009). Our results fit within these observations and add to the list of many perturbations that evoke a SKN-1 mediated response.

Importantly, amino catabolism pathways are implicated in disease progression and cancer treatment. A previous study has shown that perturbation of this pathway decreases sensitivity to the chemotherapeutic methotrexate and increasing flux through this pathway has been proposed to increase methotrexate efficacy in patients (Kanarek et al., 2018). While simple dietary intervention is appealing, our understanding of the consequences of catabolite buildup remains incomplete. Indeed, one study indicates that histidine supplementation can cause hepatic enlargement in patients with liver disease (Holeček, 2020). Moreover, in type I tyrosinemia, tyrosine catabolite buildup is thought to be a main source of damage to proteins and DNA, contributing to pathology (Ferguson et al., 2010). We observe that histidine catabolites can also signal to effectors, such as SKN-1, to modulate physiology. Thus, further studies to uncover the clear role of catabolite intermediates as important modulators of cell signaling is at the forefront of understanding human disease.

4-Imidazolone-5-Propanoate (IP) as a signaling catabolite

Enzymes of the histidine catabolism pathway are highly conserved from bacteria to humans (Bender, 2012). Interestingly, mutations in the conserved IPase in *Klebsiella aerogenes* are innocuous unless supplemental histidine is added and upstream enzymes are active, in which

case the bacteria are poisoned and fail to grow (Boylan and Bender, 1984). This phenotype bears striking resemblance to the phenotype observed here, in which *C. elegans* mutants for the IPase, *amdh-1,* show exaggerated phenotypes when supplemented with histidine, dependent on the upstream enzymes *haly-1* and *uroc-1*. To date, no direct experimentation has shown the toxicity of this catabolite, likely due to the short half-life of IP (Bowser Revel and Magasanik, 1958; Rao and Greenberg, 1961). IP may either directly or indirectly activate SKN-1 through a breakdown product, production of oxidative stress or through a distinct mechanism. Indeed, 4-imidazolones have previously been shown to cause oxidative stress and make up many advanced glycation end-products (AGEs), biomarkers that correlate with aging and metabolic disease (Niwa et al., 1997; Omar et al., 2018).

Requirements of SKN-1 activation in *amdh-1* mutants

To date, the MAPK signaling pathway has been reported to control nearly all instances of SKN-1 activation in *C. elegans* (Blackwell et al., 2015)**.** Here we report a SKN-1 transcriptional response to altered histidine catabolism that is independent of conserved MAPK components *sek-1* and *pmk-1*. Although the identity of upstream signaling components remain elusive, several kinases known to influence SKN-1 activation remain as candidates downstream of the signaling catabolite (Kell et al., 2007). Notably, we found that knockdown of *gcn-2* partially suppressed SKN-1 activation in *amdh-1* mutants. *gcn-2* is a conserved protein kinase which functions in the integrated stress response (ISR) (Pakos-Zebrucka et al., 2016). Interestingly, the homolog of SKN-1, NRF2, has known functions in regulating the transcription of ATF4, the core effector of the ISR, in mammals (Pakos-Zebrucka et al., 2016). Moreover, the *gcn-2* inhibitor, *impt-1,* extends the lifespan of *C. elegans* and requires SKN-1, highlighting potential interactions between *gcn-2*, the ISR and SKN-1. Further studies are needed to determine the entirety of the signaling cascade that culminates in the activation of SKN-1 upon metabolic perturbations, as the partial dependence of *gcn-2* suggests other factors are involved.

We also found that *suco-1* is also required for SKN-1 activation in *amdh-1* mutants. *suco-1* is a homolog of the SLP1 protein in yeast, which is hypothesized to participate in protecting nascent proteins from degradation during folding in the ER (Zhang et al., 2017). Previous work has identified UPR^{ER} components such as *ire-1* and *hsp-4* in the transcriptional response to oxidants arsenite and tBOOH (Glover-Cutter et al., 2013). If *suco-1* functions in a similar capacity in *C. elegans* as it does in yeast, this could implicate other ER protein homeostasis pathways in the regulation of SKN-1. Indeed, an ER-associated isoform of SKN-1, SKN-1A, is known to be a monitor of proteasome function and may modulate crosstalk between the ER and SKN-1 (Lehrbach et al., 2017). Interestingly, the human ortholog of *suco-1*, *SUCO*, has been shown to be required for survival of cancer cells that harbor *KEAP1* mutations, suggesting a conserved requirement for this regulator in SKN-1/NRF2 related phenotypes (Romero et al., 2020).

Activation of SKN-1 initiates a physiological trade off

Titration of SKN-1 expression is important for the pro-longevity nature of this transcription factor. Moderate overexpression of SKN-1 or mutation of the negative regulator *wdr-23* extends the lifespan of *C. elegans,* while hypomorphic mutants or worms treated with *skn-1* RNAi exhibit a shortened lifespan (Grushko et al., 2021; Ganner et al., 2019; Tullet et al., 2017; Tang and Choe, 2015; Tullet et al., 2008). However, gain-of-function animals with constitutive

expression of SKN-1 and animals containing high-copy arrays of SKN-1 exhibit a mild decrease in lifespan (Paek et al., 2012; Tullet et al., 2008). Additionally, activation of SKN-1 is beneficial for oxidative stress survival while detrimental to survival under other conditions such as heat, ER or mitochondrial stress (Deng et al., 2020). SKN-1 activation upon metabolic perturbation, as shown here, provides short term benefit to survive oxidative stress but comes at the cost of sensitivity to heat and ER stress. This may represent a physiological trade off, where SKN-1 prioritizes the allocation of cellular resources to defend against a perceived threat at the cost of sensitivity to other perturbations. Identification and study of the physiologically relevant consequences of SKN-1 activation will be crucial to understanding how modulation of this master transcription factor may be leveraged to affect human disease.

Chapter 2.3: Figures

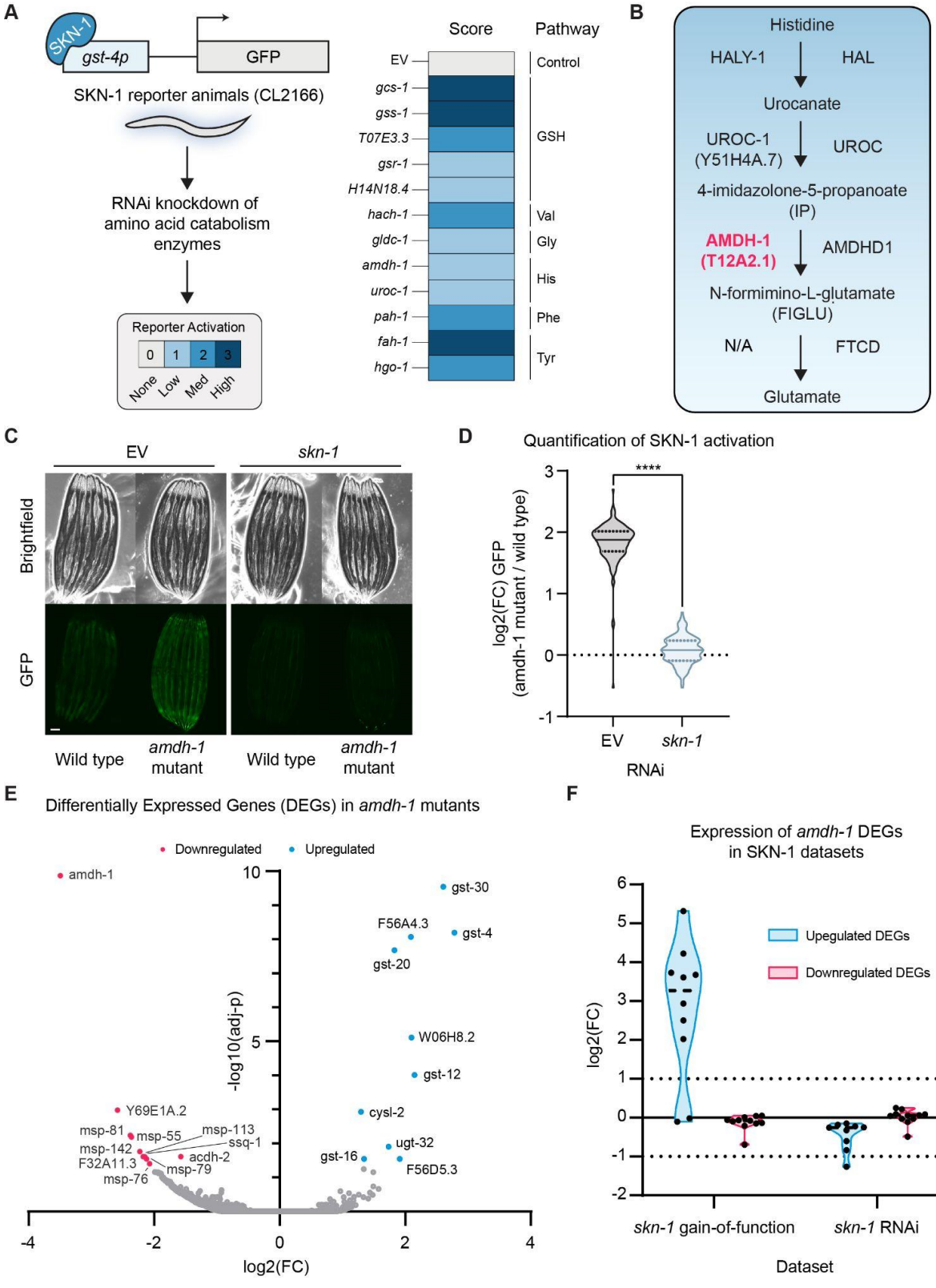

Figure 1: Perturbation of histidine catabolism activates SKN-1

(A) Experimental scheme of RNAi screen to uncover amino acid catabolism enzymes that affect SKN-1 activation (left), and scores of tested genes (right). RNAi knockdown of genes that suppressed the reporter were scored but not included (Table 1). (B) Enzymes and intermediates involved in the histidine catabolism pathway, in *C. elegans* (left) and humans (right) ("N/A" represents no identified *C. elegans* enzyme for this step). (C) Fluorescent images of SKN-1 transcriptional reporter, *gst-4p::GFP,* in wild-type or mutant backgrounds on RNAi Scale bar, 100 μm (D) Quantification of SKN-1 activation (*amdh-1* mutant normalized to median of wild type) from (C), Data are representative of n = 3 biological replicates, n > 121 animals per replicate, **** = $P < 0.0001$ using a Mann-Whitney two-tailed test. (E) Volcano plot of genes in *amdh-1(uth29)* compared to N2 control animals. Differentially expressed genes (DEGs) shown in red (downregulated) and blue (upregulated), adjusted-$p < 0.05$ (F) Meta analysis of DEGS from *amdh-1(uth29)* mutants in gain of function *skn-1(lax188)* and *skn-1* RNAi datasets(Nhan et al., 2019; Steinbaugh et al., 2015).

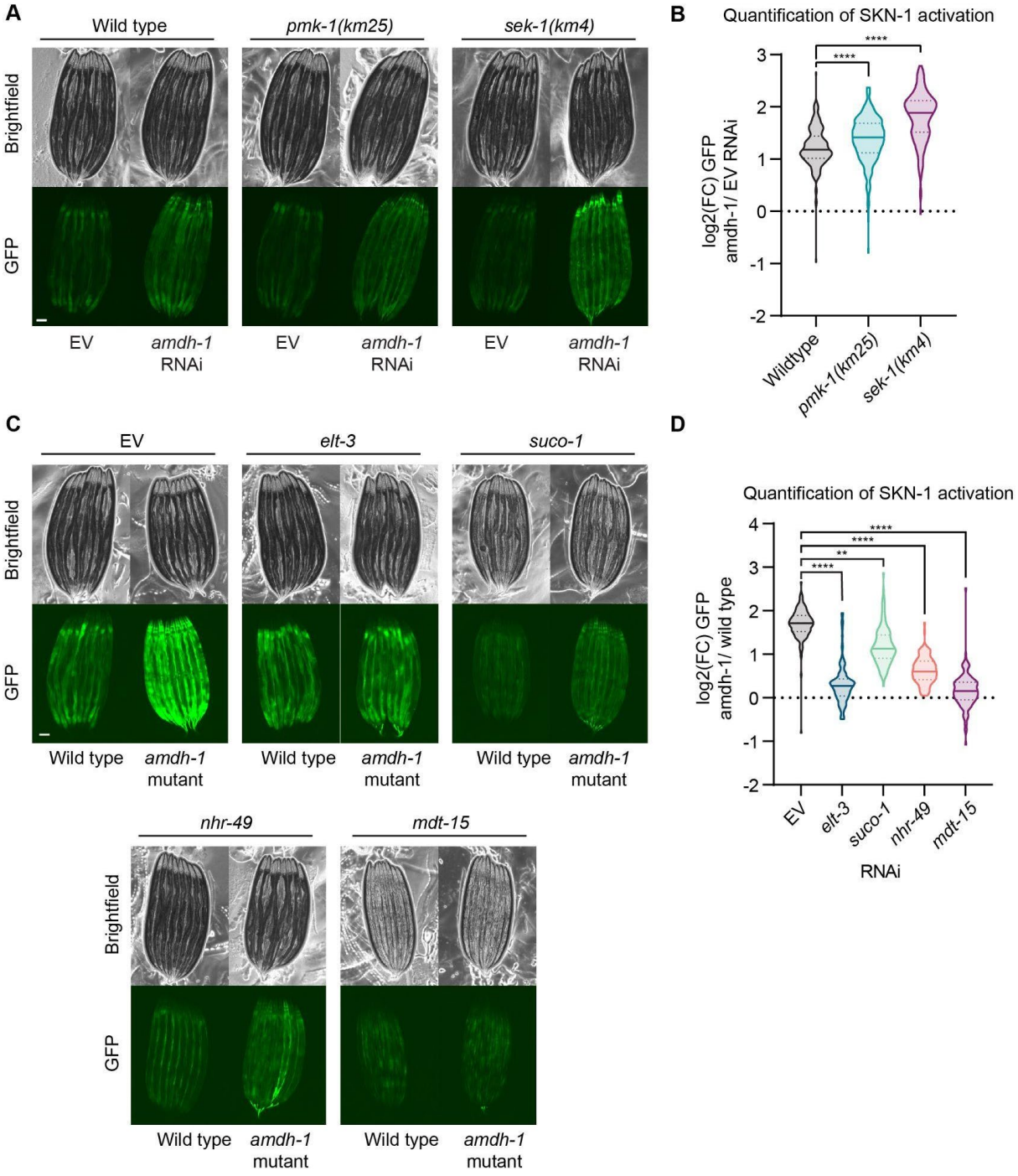
A
Wild type
pmk-1(km25)
sek-1(km4)
Brightfield
GFP
EV
amdh-1 RNAi
B
Quantification of SKN-1 activation
log2(FC) GFP amdh-1/ EV RNAi
Wildtype
pmk-1(km25)
sek-1(km4)
C
EV
elt-3
suco-1
Wild type
amdh-1 mutant
nhr-49
mdt-15
D
Quantification of SKN-1 activation
log2(FC) GFP amdh-1/ wild type
EV
elt-3
suco-1
nhr-49
mdt-15
RNAi

Figure 2: Genetic requirements of SKN-1 activation in *amdh-1* mutants

(A) Fluorescent images of SKN-1 reporter animals in a wild type, *sek-1(km4)* or *pmk-1(km25)* mutant animals fed *amdh-1* RNAi. Scale bar, 100 μm. (B) Quantification of SKN-1 activation (*amdh-1* RNAi normalized to median of EV) from (A), Data shown are representative of n = 3 biological replicates with n > 172 animals per condition for each replicate. **** = $P < 0.0001$ using a one-way ANOVA. (C) Fluorescent images of SKN-1 reporter animals in a wild type or *amdh-1(uth29)* mutant background fed RNAi targeting *elt-3*, *suco-1, nhr-49,* and *mdt-15*. Scale bar, 100 μm. (D) Quantification of SKN-1 activation (*amdh-1* mutant normalized to median of wild type) from (C), Data shown are representative of n = 3 biological replicates with n > 88 animals per condition for each replicate. ** = $P < 0.01$, **** = $P < 0.0001$ using a one-way ANOVA.

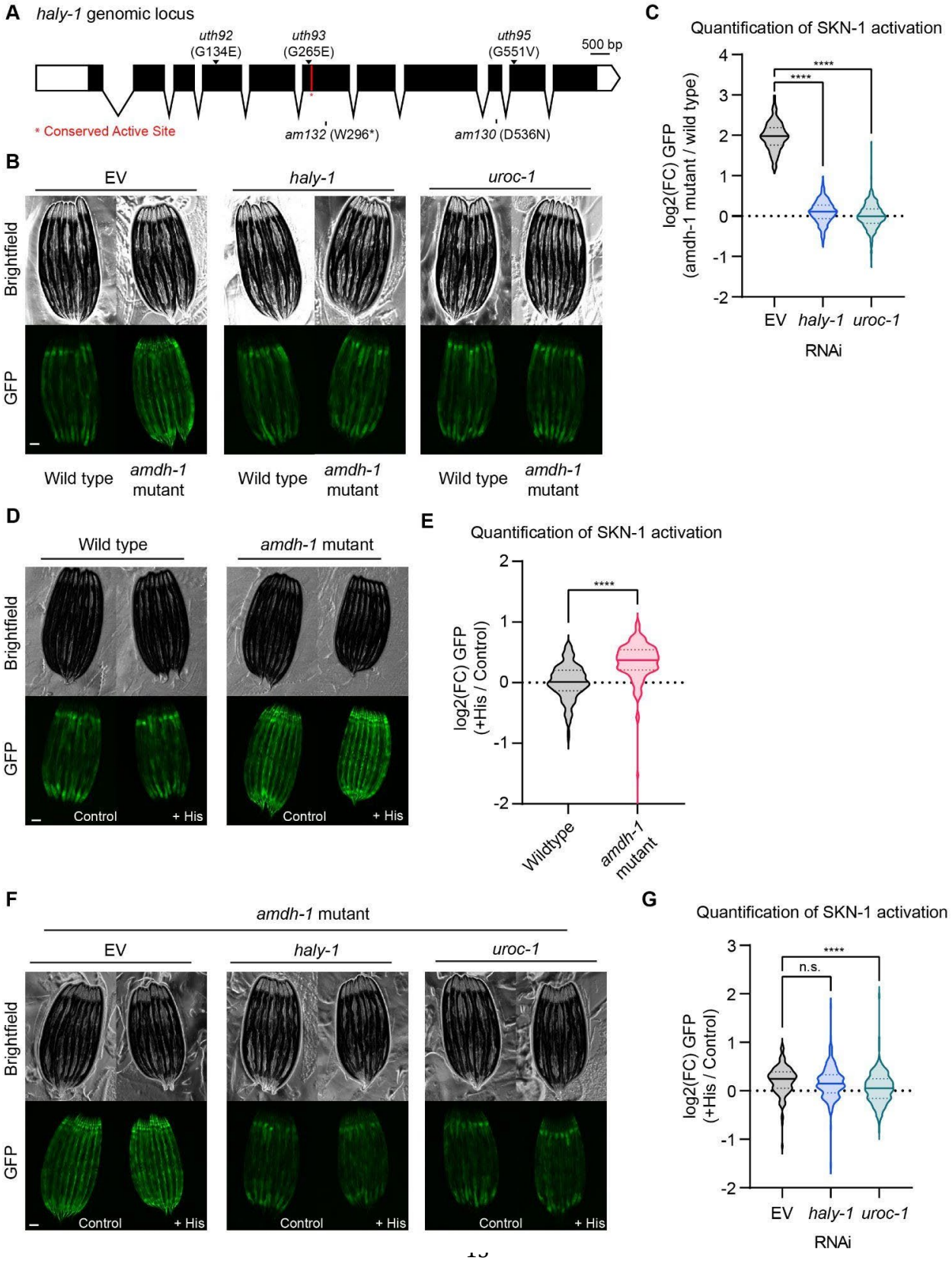
A
haly-1 genomic locus
uth92 (G134E)
uth93 (G265E)
uth95 (G551V)
500 bp
* Conserved Active Site
am132 (W296*)
am130 (D536N)
B
EV
haly-1
uroc-1
Brightfield
GFP
Wild type
amdh-1 mutant
C
Quantification of SKN-1 activation
log2(FC) GFP (amdh-1 mutant / wild type)
****
EV
haly-1
uroc-1
RNAi
D
Wild type
amdh-1 mutant
Control
+ His
E
Quantification of SKN-1 activation
log2(FC) GFP (+His / Control)
Wildtype
amdh-1 mutant
F
amdh-1 mutant
G
Quantification of SKN-1 activation
n.s.

Figure 3: Activation of SKN-1 likely proceeds through a metabolic intermediate

(A) Schematic of *haly-1* genomic locus labeling novel alleles from EMS screen (top, arrows). A conserved active site is labeled in red and two existing alleles are labeled (bottom). Scale bar, 500 bp. (B) Fluorescent images of SKN-1 reporter animals in a wild type or *amdh-1(uth29)* mutant background fed RNAi targeting *haly-1* and *uroc-1*. Scale bar, 100 μm. (C) Quantification of SKN-1 activation (*amdh-1* mutant normalized to median of wild type) from (B), Data shown are representative of n = 3 biological replicates with n > 250 animals per condition for each replicate. **** = P < 0.0001 using a one-way ANOVA. (D) Fluorescent images of SKN-1 reporter animals in a wild type or *amdh-1(uth29)* mutant background with (+ His) or without (control) 10mM histidine added to the media. Scale bar, 100 μm. (E) Quantification of SKN-1 activation (+His normalized to median of control) from (D), Data shown are representative of n = 3 biological replicates with n > 141 animals per condition for each replicate. **** = P < 0.0001 Mann-whitney U test. (F) Fluorescent images of SKN-1 reporter animals in an *amdh-1(uth29)* mutant background fed RNAi with or without 10mM histidine added to the media. Scale bar, 100 μm. (G) Quantification of SKN-1 activation (+His normalized to median of control) from (F), Data shown are representative of n = 3 biological replicates with n > 193 animals per condition for each replicate. **** = P < 0.0001 one-way ANOVA.

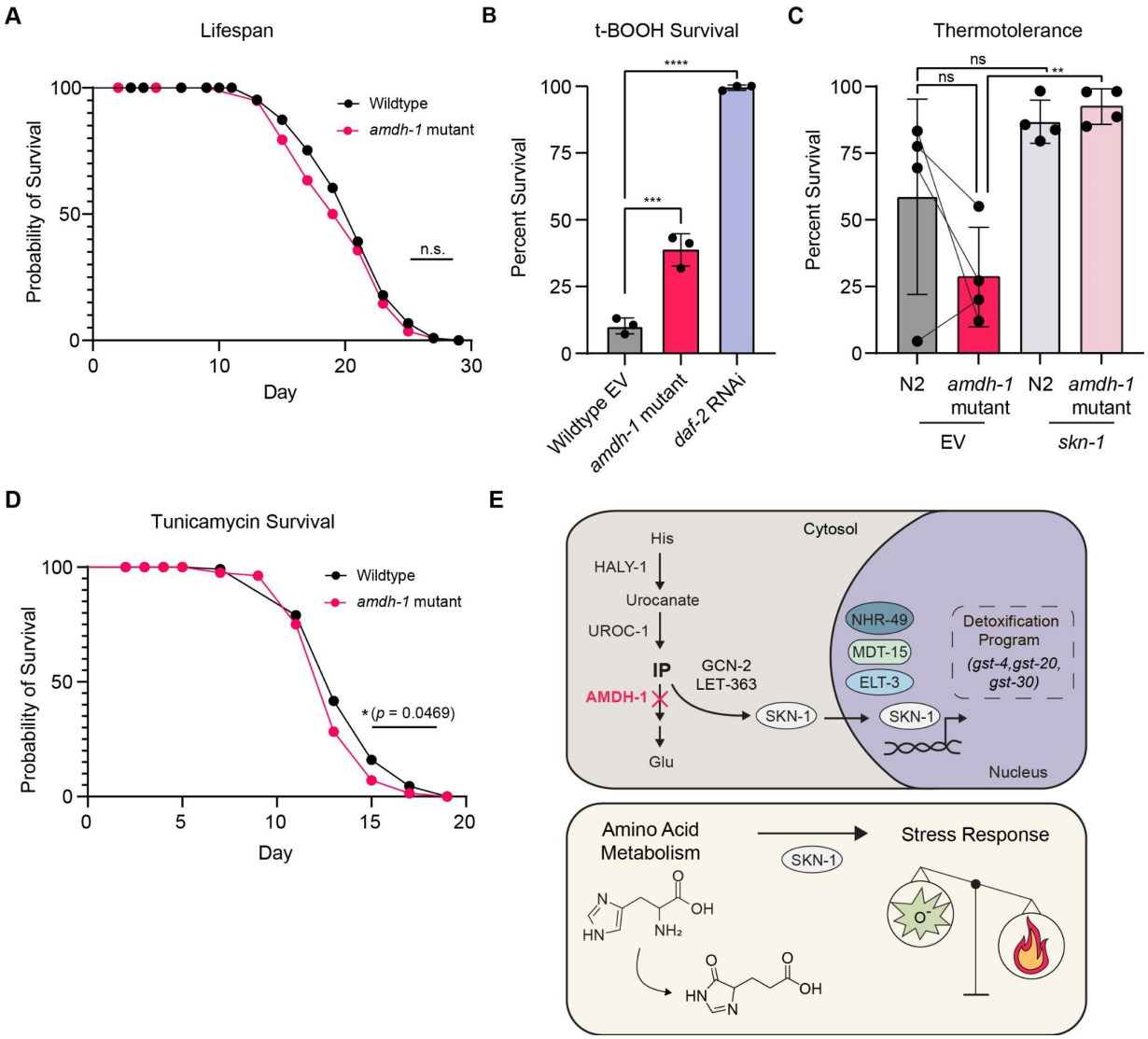
A
Lifespan
Probability of Survival
Day
Wildtype
amdh-1 mutant
n.s.
B
t-BOOH Survival
Percent Survival
Wildtype EV
amdh-1 mutant
daf-2 RNAi
C
Thermotolerance
Percent Survival
N2
amdh-1 mutant
EV
skn-1
D
Tunicamycin Survival
Probability of Survival
Day
* (p = 0.0469)
E
Cytosol
His
HALY-1
Urocanate
UROC-1
IP
AMDH-1
GCN-2
LET-363
Glu
SKN-1
NHR-49
MDT-15
ELT-3
Detoxification Program
(gst-4,gst-20, gst-30)
Nucleus
Amino Acid Metabolism
Stress Response

Figure 4: Physiological consequences of SKN-1 activation in *amdh-1* mutants

(A) Survival of wild-type animals (N2) and *amdh-1(uth29)* mutant worms at 20°C. Each data point represents one biological replicate of n > 40. One-way ANOVA with Šídák's multiple comparisons test, ** = P < .01. (B) Survival of animals on plates containing 7.5mM t-BOOH for 16 hours. One-way ANOVA with Šídák's multiple comparisons test, *** = P < 0.001, **** = P < 0.0001 (C) Thermotolerance of animals shifted to heat shock temperature (34°C) for 14-15 hours. Solid lines connecting points represent replicates complete on the same day to show the relative trend of thermotolerance between wild type and mutant animals. One-way ANOVA with Šídák's multiple comparisons test, ** = P < .01 (D) Survival of animals on 25ng/µL tunicamycin plates (E) Schematic of findings. *Top* - Perturbation of histidine catabolism via *amdh-1* mutation leads to a buildup of a catabolite that, directly or indirectly, activates a transcriptional program of detoxification enzymes driven by SKN-1. This response requires nuclear factors NHR-49, MDT-15 and ELT-3. *Bottom* - Activation of SKN-1 via perturbation of histidine catabolism leads to a physiological tradeoff of increased oxidative stress resistance and decreased heat tolerance.

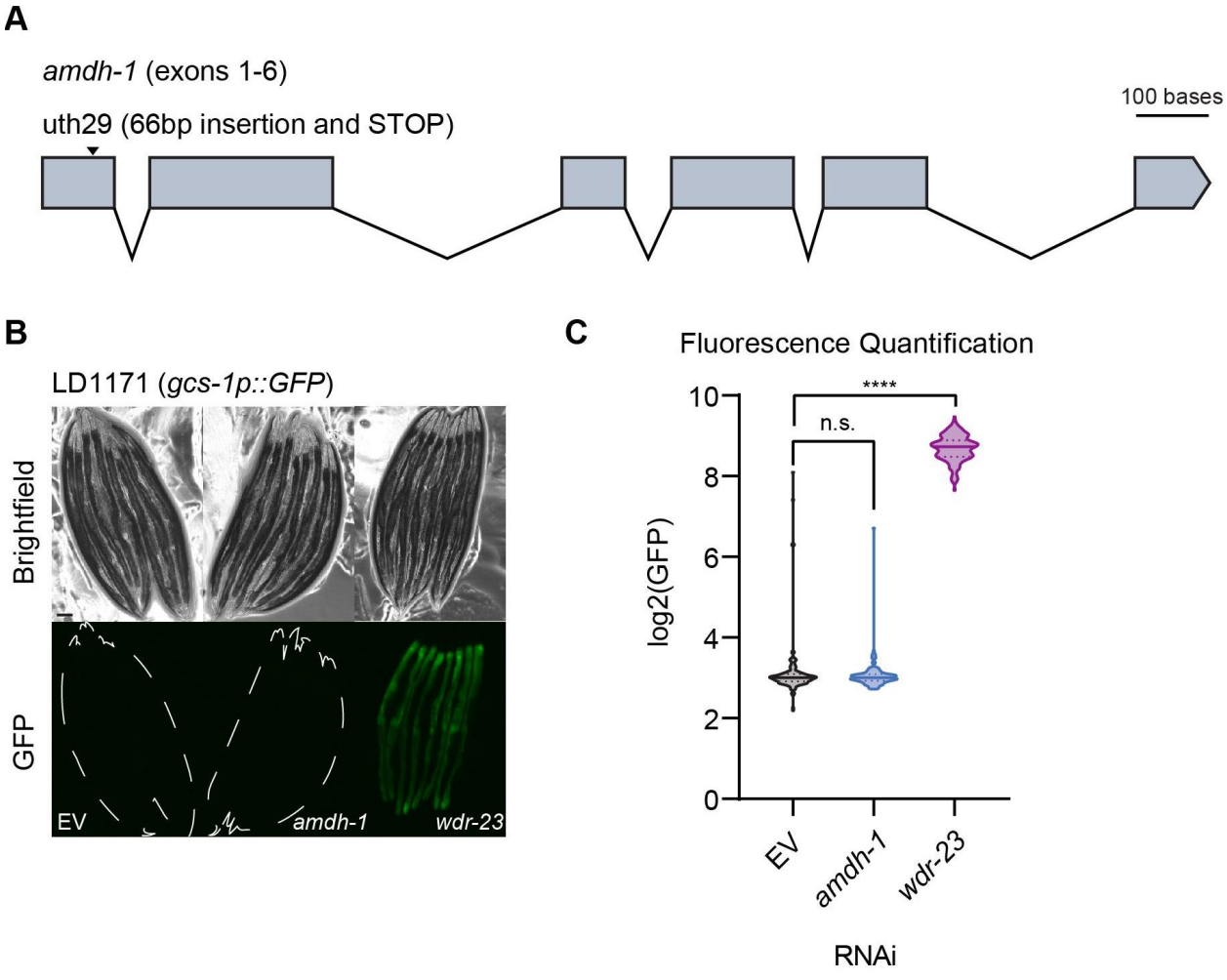

Supplemental Figure 1

(A) Schematic of *amdh-1/T12A2.1* genomic locus showing the location of allele *uth29* engineered using CRISPR/Cas9 (top, arrow). Scale bar, 100 bases. (B) Fluorescent images of SKN-1 reporter worms (*gcs-1p::GFP)* fed RNAi targeting *amdh-1* and *wdr-23*. Scale bar, 100 μm. (C) Quantification of (B)*,* Data shown are representative of n = 4 biological replicates with n > 60 animals per condition for each replicate. **** = $P < 0.0001$, n.s. = not significant using a one-way ANOVA non-parametric test (Kruskal-wallis).

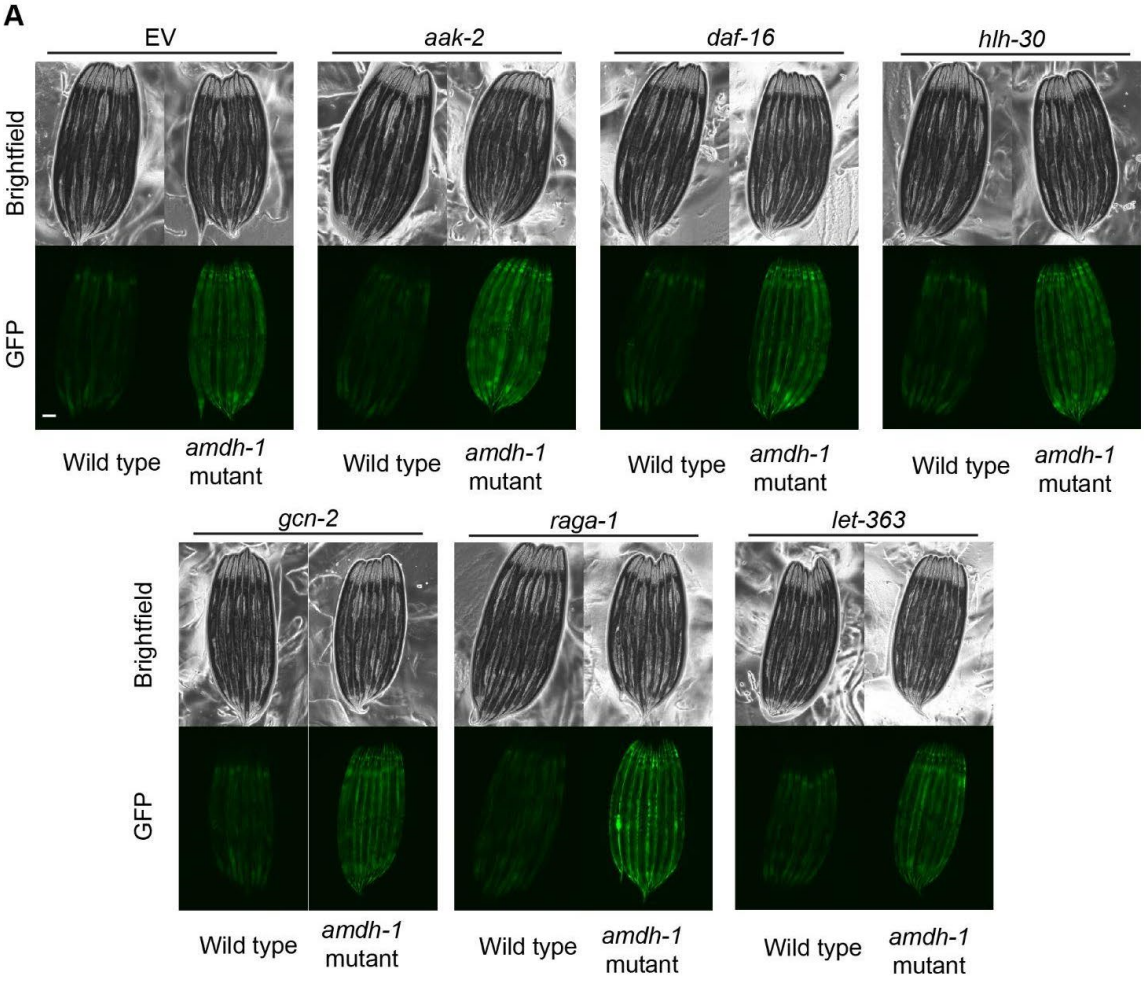

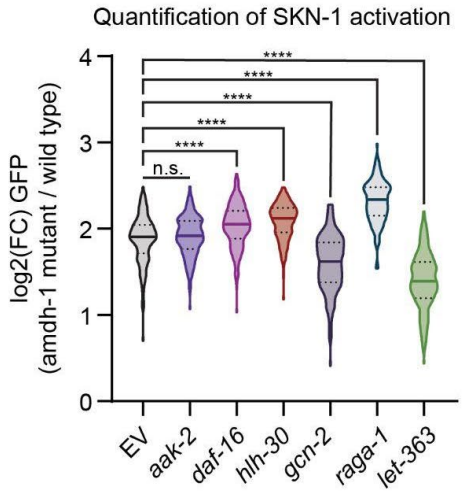

C

Allele	Gene	Mutation
uth89	*skn-1*	A514T
uth94	*elt-3*	Q128*
uth112	*suco-1*	A429M
uth92	*haly-1*	G134E
uth93	*haly-1*	G265E
uth95	*haly-1*	G551V

Supplemental Figure 2

(A) Fluorescent images of SKN-1 reporter animals (*gst-4p::GFP)* fed RNAi targeting. Scale bar, 100 μm. (B) Quantification of (A), Data shown are representative of n = 2 biological replicates with n > 123 animals per condition for each replicate. (C) Table of causative mutations mapped using whole genome sequencing.

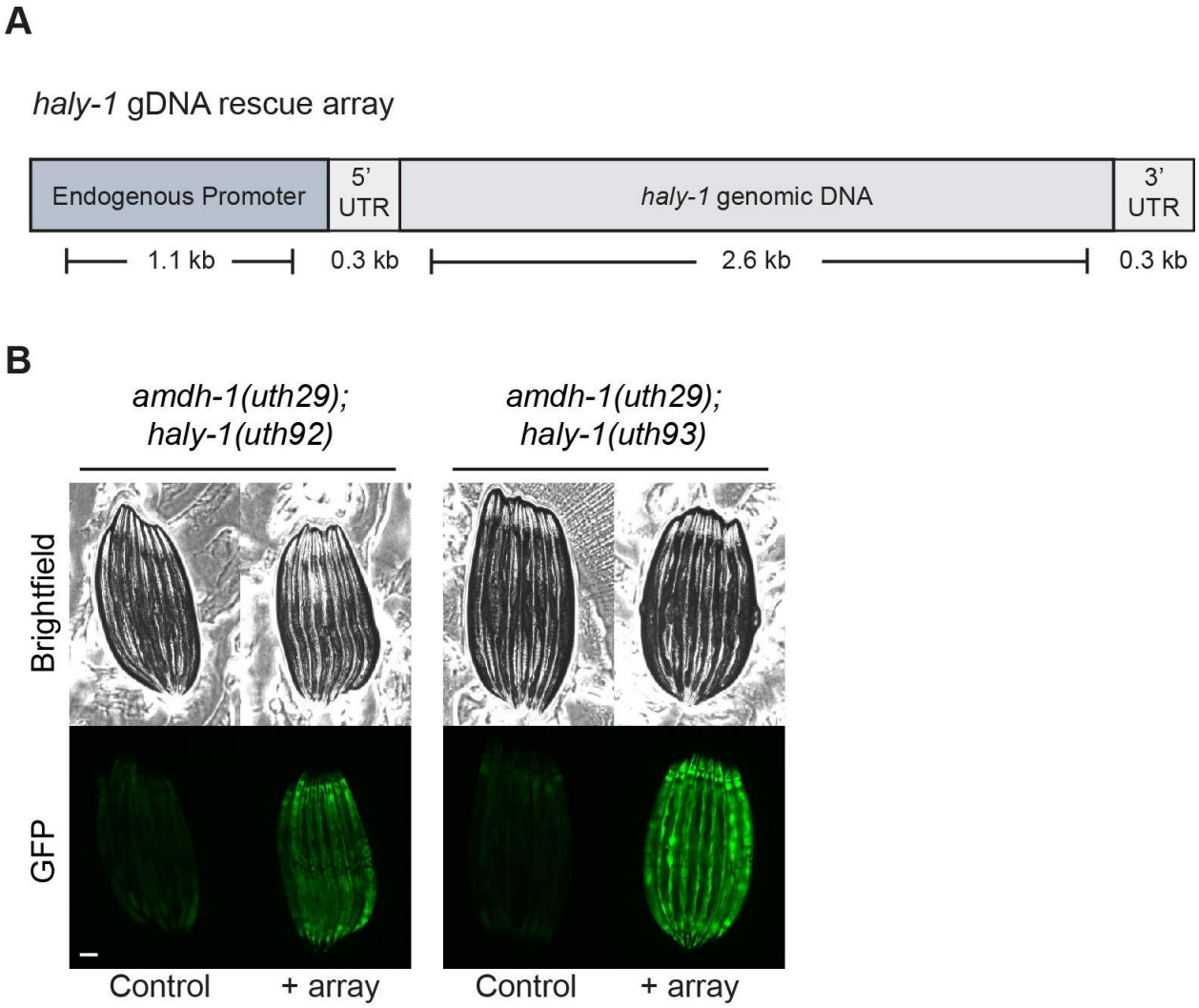

Supplemental Figure 3

(A) Schematic of *haly-1* genomic DNA (gDNA) rescue array used for genetic rescue experiments to confirm causality (B) Fluorescent images of *haly-1; amdh-1* double mutants with or without *haly-1* gDNA rescue array. Scale bar, 100 μm.

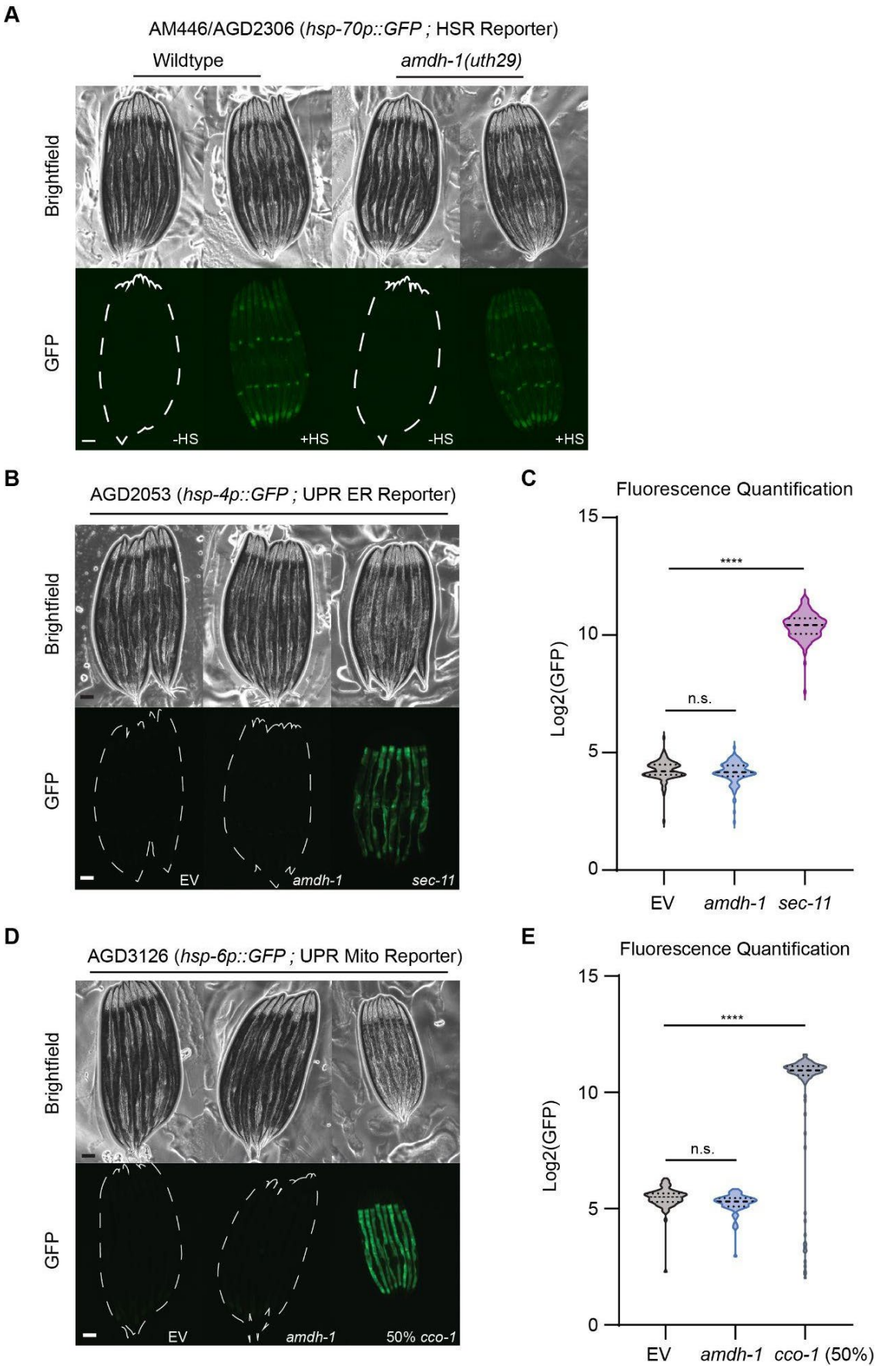
A
AM446/AGD2306 (hsp-70p::GFP ; HSR Reporter)
Wildtype
amdh-1(uth29)
Brightfield
GFP
-HS
+HS
-HS
+HS
B
AGD2053 (hsp-4p::GFP ; UPR ER Reporter)
Brightfield
GFP
EV
amdh-1
sec-11
C
Fluorescence Quantification
Log2(GFP)
15
10
5
0
****
n.s.
EV
amdh-1
sec-11
D
AGD3126 (hsp-6p::GFP ; UPR Mito Reporter)
Brightfield
GFP
EV
amdh-1
50% cco-1
E
Fluorescence Quantification
Log2(GFP)
15
10
5
0
****
n.s.
EV
amdh-1
cco-1 (50%)

Supplemental Figure 4

(A) Fluorescent images of heat shock response (HSR) reporter animals (hsp-70p::GFP) with or without heat shock treatments (34C) in wild type and amdh-1(uth29) mutant animals. Data shown are representative of n = 3 biological replicates. Scale bar, 100 μm. (B) Fluorescent images of a reporter of the unfolded protein response of the ER (UPR ER) animals (*hsp-4p::GFP)* fed RNAi. Scale bar, 100 μm. (C) Quantification of (B), Data shown are representative of n = 3 biological replicates with n > 50 animals per condition for each replicate. **** = P < 0.0001, n.s. = not significant using a one-way ANOVA non-parametric test (Kruskal-wallis) (D) Fluorescent images of UPR Mito reporter animals (*hsp-6p::GFP)* fed RNAi. Scale bar, 100 μm. (E) Quantification of (D), Data shown are representative of n = 3 biological replicates with n > 50 animals per condition for each replicate. **** = P < 0.0001, n.s. = not significant using a one-way ANOVA non-parametric test (Kruskal-wallis)

Chapter 3: Other factors involved in SKN-1 metabolic surveillance

We have demonstrated that SKN-1 acts as a metabolic surveillance factor; it can be activated in the face of metabolic perturbations, namely deletion of the conserved amidohydrolase of the histidine catabolism pathway, *amdh-1*, to evoke a transcriptional response of detoxification enzymes. We found that this response is partially dependent on key nutrient regulators, *gcn-2* and *let-363/mTORC2* as well as oxidative stress regulators *elt-3, nhr-49* and *mdt-15.* SKN-1 is thought to be activated primarily via phosphorylation by the MAPK signaling pathway in response to oxidative stress such as arsenite, paraquat and tert-butyl hydroperoxide (Blackwell et al., 2015; Inoue et al., 2005). Interestingly, in response to mutations in the histidine catabolism pathway, SKN-1 does not depend on MAPK components MAPKK, *sek-1*, or P38/MAPK, *pmk-1* (Figure 2a,b). Indeed, novel kinases have been identified that control SKN-1 activation in the face of oxidative stress, such as *nekl-2*, *ikkε-1*, *mkk-4* and *pdhk-2*, although the requirement for them in other SKN-1 mediated processes are less worked out (Kell et al., 2007).

To gain further mechanistic insight into the pathways involved in SKN-1 metabolic surveillance, we performed a series of targeted RNAi screens knocking down key kinases, phosphatases, chromatin genes and regulators of the TCA cycle to test whether these genes are required for SKN-1 activation. Kinases, phosphatases and chromatin regulators are integral to many cellular signaling pathways. Therefore, genes identified from these screens will inform us of novel regulatory inputs to SKN-1 signaling pathways as it relates to the interplay between this important transcription factor and metabolism.

Chapter 3.1: Results

Kinases, phosphatases and chromatin associated proteins are critical to cellular signaling cascades and gene expression. These proteins represent important regulatory nodes that are essential to virtually all cellular processes. Furthermore, many of these regulators belong to distinct pathways, the discovery of which may shed light on novel regulatory inputs to SKN-1. To test for the requirements of signaling between the histidine catabolism pathway and SKN-1, and to find novel regulatory nodes of SKN-1 activity, we used sequence verified RNAi sub-libraries consisting of nearly 900 clones targeting a wide array of signaling proteins from phosphatases, kinases, chromatin associated proteins and TCA cycle genes (Figure 5a). Using these RNAi sub-libraries, we assessed SKN-1 activity in *amdh-1* mutant animals by measuring the GFP fluorescence of the SKN-1 reporter construct in these animals (Figure 5b). Hits from these screens were then analyzed using pathway analysis and STRING, a database used to identify and predict interactions between proteins, in order to identify any pathways or potential interactors of our hits that control SKN-1 activity in the face of metabolic perturbations (Figure 5b).

From our screens, we identified 27 hits that suppress SKN-1 activation in *amdh-1* mutants when knocked down. These hits encompass all 5 sub-libraries: chromatin (*lin-41*, *cbp-1*, *lex-1*, *his-34, cec-1*, *lin-61*, *lin-40*, *his-65*, *his-43* and *his-57*), kinase (*kin-19, kin-2, nekl-2, let-754, ppk-1, pkc-3* and *alh-13*), MAPK (*vhp-1*), phosphatase (*hpo-8, gfi-2, mel-11, F54C8.4* and *tax-6*) and TCA cycle (*dlst-1* and *ogdh-1*) (Figure 6a, Tables 2-6). Furthermore, using pathway enrichment analysis, we found that these genes are significantly enriched for a few pathways including WNT

signaling (*cbp-1, tax-16* and *kin-19*), TCA cycle (*dlst-1* and *ogdh-1*), MAPK signaling (*tax-6* and *vhp-1*), among others (Figure 6b).

STRING is a database that aims to curate experimentally determined and bioinformatically predicted protein–protein interactions into a functionally associated network (Szklarczyk et al., 2021). We utilized this database to determine if genes identified from our screen are known or predicted to interact with each other, and to predict other protein interactors. Four clusters of nodes were found, one of which contained the histone proteins discovered in our screen, suggesting that these proteins may be interactors (Figure 6c). Finally, STRING allows for predictions of interacting proteins of the list of hits from the screen. From this, we identified *D1005.1*/*acly-1*, *acly-2*, *dld-1, kin-1* and *ZK836.2/ogdh-2* as potential interactors of genes identified in our screen, which may be interesting targets to follow up on to further uncover the regulatory mechanisms of SKN-1 (Figure 6c). Of these, *kin-1* was already screened and showed suppression of SKN-1 activity in 1 of 2 replicates, suggesting that it may indeed play a role in SKN-1 regulation and further validating the predictive capabilities of this method (Table 6). Taken together, our RNAi screens have identified many more potential regulators of SKN-1 metabolic function and therefore serve as a starting point for more in-depth study of this process.

Chapter 3.2: Discussion

Upon discovering that SKN-1 can respond to disruption of key metabolic pathways, namely amino acid catabolism, we were interested in determining the requirements of this activation. We found that, although this response required nuclear factors involved in detoxification gene expression, MAPK regulators *pmk-1* and *sek-1* were dispensable for the activation of SKN-1 in *amdh-1* mutants (Frankino et al., 2022). This suggested that other previously undescribed regulators may influence SKN-1 activity in response to metabolic perturbation. Upon screening our RNAi sub-libraries, which consisted of almost 900 genes, we found genes with previous implications in SKN-1 signaling. One interesting hit that stands out is *vhp-1,* a MAPK phosphatase that has been proposed to be a negative regulator of PMK-1 in response to PA14 exposure (Kim et al., 2004; Papp et al., 2012). PMK-1 can directly phosphorylate SKN-1, at residues S74 and S340, and is thought to do this in response to oxidative stress after phosphorylation by its upstream kinase, SEK-1, in *C. elegans* (Inoue et al., 2005). Therefore, a reasonable hypothesis would be that *vhp-1* knockdown might de-repress PMK-1, which would activate SKN-1 signaling. In our screen, however, knockdown of *vhp-1* suppressed SKN-1 reporter animals in an *amdh-1* mutant background, suggesting that this phosphatase is a positive regulator of SKN-1 activity. These data further support our other findings that PMK-1 and SEK-1 are not required for SKN-1 activation in *amdh-1* mutants, so it is not surprising that knockdown of a negative regulator does not function in the same direction (Frankino et al., 2022). Notably, Papp and colleagues also noticed that *vhp-1* knockdown had no effect on *gcs-1* reporter on OP50, suggesting that the requirement of this phosphatase to activate SKN-1 signaling via PMK-1 may be specific to pathogen infection and not metabolic perturbations (Papp et al., 2012).

The finding that *vhp-1* is an activator of SKN-1 activity uncovers the interesting observation that this phosphatase is among the first of its kind identified to control SKN-1 processes in response to metabolic perturbation. One possibility is that this interaction is direct, and that VHP-1

dephosphorylates an inhibitory phosphorylation site on SKN-1. To our knowledge, this would be the first example of a phosphatase directly modulating SKN-1 activity in this manner. Indeed, SKN-1 can be inhibited via phosphorylation by kinases such as *gsk-3, akt-2* and *sgk-1* (Blackwell et al., 2015). Since most of these phosphorylation sites are well characterized, they therefore represent interesting residues to interrogate in respect to VHP-1/SKN-1 interactions. Another possibility includes an indirect interaction between VHP-1 and one of these inhibitory kinases, where VHP-1 may dephosphorylate them, rendering them inactive. Besides the three aforementioned kinases, there have been other inhibitory kinases discovered, although it is unclear if the nature of these interactions is direct or indirect (Papp et al., 2012). Finally, it has not escaped our attention that a previous study, utilizing ChIP-seq data, found that ELT-3 can bind in the coding region of *vhp-1* (Shao et al., 2013). This may indicate that *vhp-1* is an important regulator of SKN-1 downstream of nuclear factors required for detoxification responses. In sum, our work expands the extent to which VHP-1 can be considered a regulator of SKN-1 and sets the foundation for further characterization of this interaction in the broader context of metabolism.

In response to stress, transcription factors, such as SKN-1, help drive gene expression programs in the nucleus. Inside the nucleus, however, DNA is wrapped around histones into chromatin, in regions that can be tightly or loosely packed (heterochromatin or euchromatin, respectively). Thus, a key challenge of transcription factors is finding and recognizing their binding sequence, usually in the promoter region of genes they control, in a crowded nuclear environment. Furthermore, DNA accessibility can be controlled by direct modification of histones such as histone acetylases and methyl transferases. Indeed, chromatin proteins are key factors in the gene expression programs in response to stress (Smith and Workman, 2012). For example, histone methyltransferase MET-2, and its cofactor LIN-65 are necessary for mitochondrial UPR activation (Tian et al., 2016). Additionally, two histone demethylases, JMJD-1.2 and JMJD-3.1, were found to be essential in both mitochondrial UPR expression programs as well as lifespan extension caused by mitochondrial signaling (Merkwirth et al., 2016). In our screen, we identified a cluster of histone genes that suppress SKN-1 activation and are experimentally determined to interact with each other (*his-57, his-34, his-43* and *his-65*) (Figure 6c). To our knowledge, these genes have not been identified to have a role in SKN-1 related gene expression and may represent novel chromatin associated proteins that help control stress responses. One limitation of this study, however, comes from the use of RNAi knockdown on genes that may be similar in sequence identity, such as histones. For example, we cannot rule out that RNAi against any one of these histone genes may also knockdown other genes with sequence similarity. Future study, using complementary approaches, will prove useful to identify chromatin proteins that can affect stress response gene expression. In addition to potentially novel regulators, we also found a previously discovered gene, *cbp-1*, known to be involved in SKN-1 signaling. *cbp-1*, an ortholog of lysine acetyltransferases CBP/P300, is a known SKN-1 interactor that is required for its nuclear localization and upregulation of stress induced genes (Ganner et al., 2019). Additionally, it was recently reported that *cbp-1* functions downstream of *jmjd-1.2* and *jmjd-3.1* to regulate the mitochondrial UPR (Li et al., 2021). It would be interesting to understand if *cbp-1* and histone genes *his-57, his-34, his-43* and *his-65* may act together to regulate SKN-1 mediated stress responses and to find other stress responses that *cbp-1* may be involved in.

Organisms generate energy from the carbohydrates, fats and proteins that they get from their diets through cellular pathways, such as the TCA cycle. The TCA cycle is a series of biochemical reactions to oxidize acetyl-CoA and produce electron carriers that are important for cellular respiration. Since *amdh-1* mutants lack an enzyme required for the catabolism of histidine into glutamate, we reasoned that TCA cycle enzymes may be important for the SKN-1 response seen in these animals. We found that knockdown of either *ogdh-1* or *dlst-1* suppresses SKN-1 activation upon disruption of histidine catabolism. *dlst-1* and *ogdh-1* are predicted to be subunits of the oxoglutarate dehydrogenase complex, which acts on substrates alpha ketoglutarate (2-oxoglutarate), CoA and NADP+ to form succinyl-CoA, CO2 and NADPH (KEGG 2021, Kanehisa et al., 2016). Intriguingly, IP, the intermediate that we predict to build up and lead to activation of SKN-1, spontaneously decays into α-ketoglutarate, a substrate of oxoglutarate dehydrogenase (KEGG 2021, Kanehisa et al., 2016). This finding suggests that the activation of SKN-1 in *amdh-1* mutants may be an indirect result of IP buildup, perhaps through accumulation of TCA cycle intermediate α-ketoglutarate. Before our study, *dlst-1* had not been previously identified as a regulator of SKN-1 mediated transcription. Rather, it was found in a screen of mitochondrial genes that, when knocked down, activate the mitochondrial UPR reporter, *hsp-6p::GFP,* and extend lifespan in *C. elegans* (Bennett et al., 2014). Although *dlst-1* RNAi activates the mitochondrial UPR, it was also reported to decrease *hsp-16.2p::GFP*, a reporter for the heat shock response. Together, these findings highlight the importance of this regulator in cellular response to stress and suggest that it may have opposing roles in distinct stress responses.

Chapter 3.3: Figures

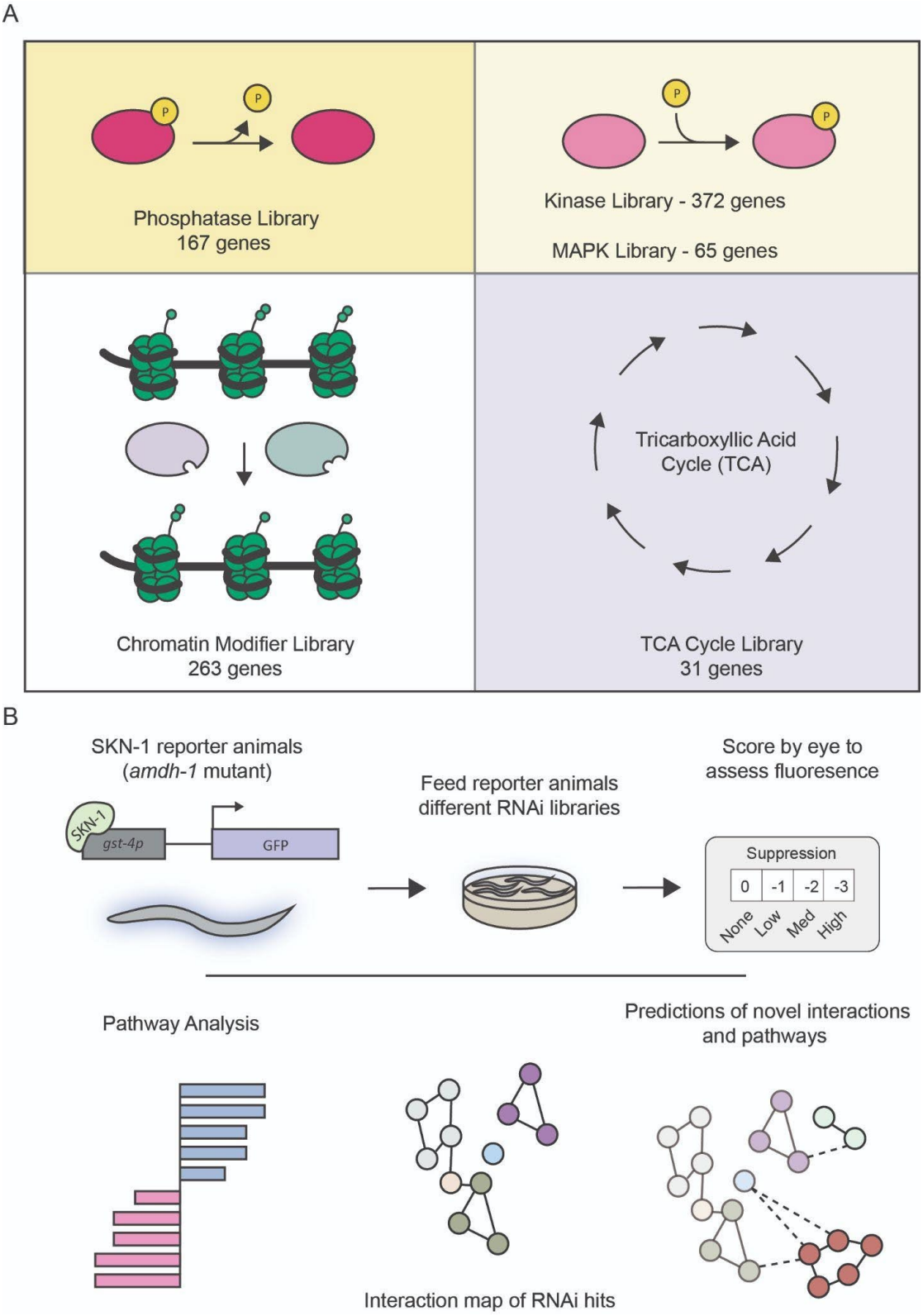

Figure 5: RNAi sub-library screening approach
(A) Existing and newly constructed RNAi sub libraries that were used to screen for the requirements of SKN-1 activation in *amdh-1* mutants (B) Schematic outlining the screening process for suppressors of SKN-1 activation (C) Additional analyses that were conducted on hits from the RNAi screens mentioned in (A) and (B)

A

Gene	Average Screen Score	
lin-41	-3	
cbp-1	-3	
lex-1	-2	
his-34	-2	
cec-1	-2	Chromatin
lin-61	-1	
lin-40	-1	
his-65	-1	
his-57	-1	
his-43	-1	
kin-19	-3	
kin-2	-3	
nekl-2	-2	
let-754	-2	Kinase
ppk-1	-1.5	
pkc-3	-1.5	
alh-13	-1	
pat-4	-1	
vhp-1	-2.83	MAPK and Ppase
T16G12.6	-2	
hpo-8	-1.5	
gfi-2	-1	PPase
mel-11	-1	
F54C8.4	-1	
tax-6	-1	
dlst-1	-2.25	TCA Cycle
ogdh-1	-2.5	

B

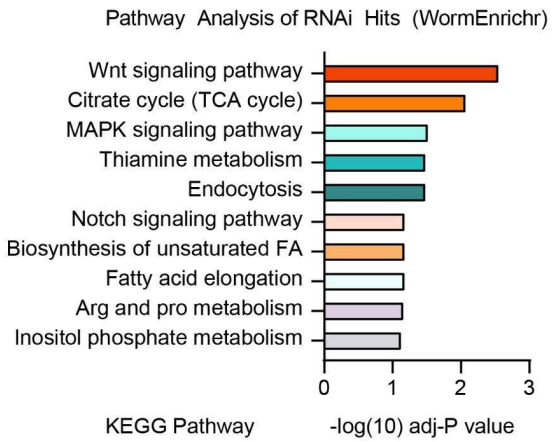

C

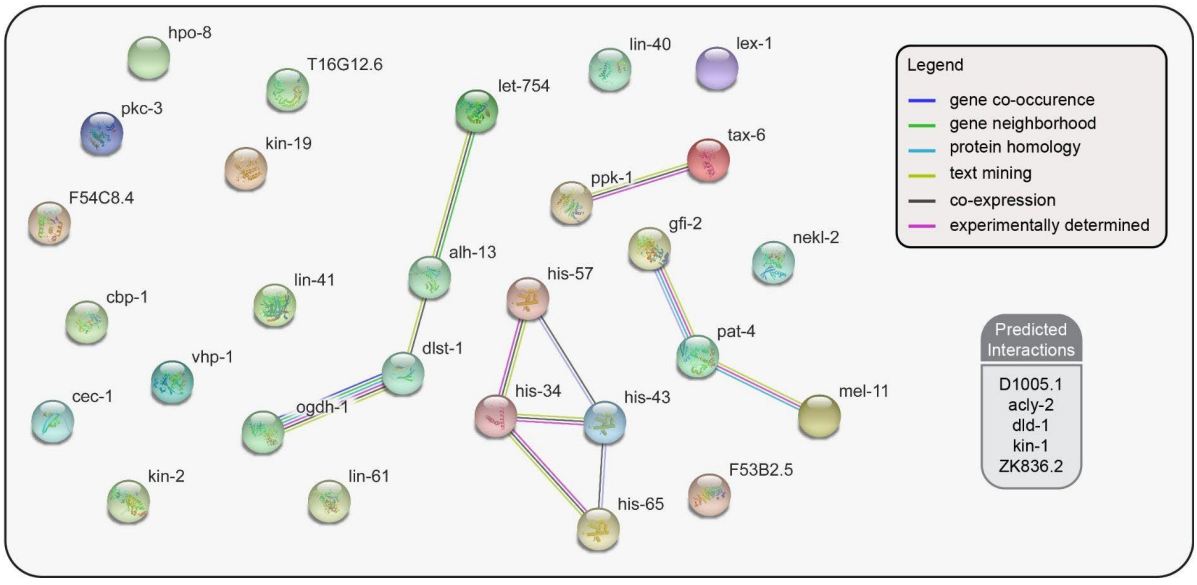

Figure 6: RNAi sublibrary screening results
(A) Hits from RNAi screening on *amdh-1* mutants for suppressors. (B) Pathway analysis of suppressors from (A) using WormEnrichr (Chen et al., 2013)

Chapter 4: Conclusions and Future Directions

Chapter 4.1: Conclusions

SKN-1 is best known for its role as a transcription factor involved in upregulating detoxification and antioxidant synthesis genes in response to a wide variety of oxidative stressors, a process known as the OxSR. Recent work has also ascribed a new role for SKN-1 in metabolic processes (Blackwell et al., 2015; Pang et al., 2014). Here, we have identified multiple amino acid catabolism pathways whose perturbation evokes a SKN-1 mediated transcriptional response. Using the histidine catabolism pathway as a model, we sought to determine the requirements and physiological consequences of SKN-1 signaling in response to the disruption of cellular metabolism.

We found that mutation of the histidine catabolism enzyme, *amdh-1*, results in a robust and specific activation of SKN-1; *gst-4p::GFP* reporter animals exhibit a ~4-fold change in activation while *gcs-1p::GFP* reporter animals show no response. Furthermore, RNA-seq analysis showed that many specific detoxification enzymes of the GST family were upregulated, genes that have been shown to change in expression in independent genetic models of SKN-1 activation and knockdown (Nhan et al., 2019; Steinbaugh et al., 2015)**.** Although most instances of SKN-1 signaling that have been investigated to date require the p38/MAPK pathway (van der Hoeven et al., 2011; Inoue et al., 2005; Tang and Pang, 2016)**,** we find that this pathway is dispensable for SKN-1 activation in *amdh-1* mutants. Instead, we observed that key nuclear factors *elt-3, mdt-15, nhr-49* and *cbp-1* were required for this response, all of which had been previously implicated in the SKN-1 mediated expression of detoxification genes (Ganner et al., 2019; Goh et al., 2014, 2018; Hu et al., 2017; Wu et al., 2016). Notably, we also found that *gcn-2* and *let-363* were partially required for SKN-1 activation in *amdh-1* mutants, suggesting that core nutrient sensing pathways may play a role in this response. Finally, through extensive screening of known kinases, phosphatases and chromatin genes, we found additional requirements for this SKN-1 signaling pathway, including *vhp-1*. Taken together, our findings suggest that SKN-1 senses and responds to perturbations of amino acid catabolism pathways and that this response is dependent on both known, and previously unidentified, components of SKN-1 signaling.

Through EMS mutagenesis screening, we identified multiple independent mutations in *haly-1*, the first enzyme in the histidine catabolism pathway, which suppresses SKN-1 activation in *amdh-1* mutants. Additionally, RNAi knockdown of *uroc-1*, the second enzyme which is immediately upstream of *amdh-1*, also suppressed SKN-1 signaling in our model. These findings suggest that histidine catabolites, metabolic breakdown products that might buildup in *amdh-1* mutants, could be responsible for SKN-1 activation. Indeed, metabolite intermediates have been proposed to affect SKN-1 signaling in multiple other studies (Fisher et al., 2008; Ravichandran et al., 2018; Tang and Pang, 2016). Supplementation of *amdh-1* mutants, but not wild-type animals, with excess histidine further activated SKN-1, dependent on the upstream enzymes, supporting a model of catabolite buildup.

Activation of SKN-1 can have both positive and negative effects on stress resistance, depending on the mechanism of activation and the stress resistance tested (Crombie et al., 2016; Deng et al., 2020). We found that while *amdh-1* mutants had no change in median lifespan, they exhibit an

increased resistance to oxidative stress with a decreased resistance to heat stress, which is completely rescued with SKN-1 knockdown. These data suggest that SKN-1 activation may result in a physiological tradeoff between stress resiliencies when activated in response to metabolic perturbations.

Together, our data suggest a model of SKN-1 signaling that includes sensing and activation mechanisms in response to disruptions of metabolism. While it is unclear whether or not this is a direct sensing mechanism, this model raises intriguing possibilities about the role SKN-1, a major transcription factor best known for its role in the OxSR, in other cellular processes. For example, the finding that intermediates from multiple amino acid catabolism pathways may activate SKN-1 highlights a key aspect of cell signaling. Intermediates may act as signals that report the state of multiple metabolic pathways simultaneously, which could be integrated by the cell to activate a main effector, SKN-1, to modulate physiology depending on the cue. If correct, this would open up a subfield of SKN-1 biology focused on finding metabolic intermediates and cell signaling cascades that affect its signaling as well as the physiological outcomes of these signaling events.

Chapter 4.2: Future Directions

The work presented in this thesis suggests a sensing and signaling mechanism that culminates in the activation of SKN-1 in response to metabolic perturbation. When histidine catabolism is disrupted, SKN-1 becomes transcriptionally active, likely due to a buildup of the catabolite IP. One important question is whether or not SKN-1 signaling is a direct or indirect result of IP accumulation. For other cases, such as the proline catabolite P5C, catabolite buildup results in SKN-1 activation in an indirect manner, via oxidative stress. Pathogen infection triggers expression changes of catabolism enzymes to activate the dual oxidase, *bli-3*, which creates ROS and activates SKN-1 through PMK-1 (Tang and Pang, 2016). Tyrosine catabolites, which may also activate SKN-1 (Fisher et al., 2008), are thought to be a form of oxidative stress, hinting at a similar indirect mechanism of activation (Jones et al., 2020). Thus, future study to interrogate the mechanism of SKN-1 activation in *amdh-1* mutants should focus on changes in oxidative stress and whether or not this activation is conserved from worms to other higher organisms such as humans. Additionally, antioxidant supplementation, such as N-acetyl cysteine (NAC) may rescue some of these phenotypes, which would support the existence of an indirect activation mechanism through ROS.

SKN-1 can respond to changes in many different metabolic pathways and can control metabolic processes, as is the case during pathogen challenge (proline catabolism and somatic lipid storage) (Nhan et al., 2019; Tang and Pang, 2016), in the absence of germline stem cells (lipid metabolism) (Steinbaugh et al., 2015), in a perceived state of starvation (starvation response) (Paek et al., 2012) as well as in many other cases (Blackwell et al., 2015). Our data show that there are many amino acid catabolism pathways that also provoke a SKN-1 response when modulated. More studies are needed that focus on (1) pathways linked to SKN-1 signaling, (2) the mechanism of these signaling events and (3) the physiological outcomes of SKN-1 activation in the context of metabolism. Additionally, identification of metabolite intermediates that can signal from these pathways to SKN-1 will be of interest to many fields and have implications outside of this field, such as in cancer biology and human disease.

Chapter 5: Materials and Methods

Strain List

Strain	SOURCE	IDENTIFIER
C. elegans: strain N2 (Bristol)	CGC	N2
C. elegans: strain LD1171: ldIs3 [gcs-1p::GFP + rol-6(su1006)]	CGC	LD1171
C. elegans: strain CL2166: dvIs19[pAG15(gst-4p::GFP::NLS)] III	CGC	CL2166
C. elegans: strain *AM446: rmIs223[pC12C8.1::GFP; rol-6(su1006) II]*	Gift from Morimoto lab (Morley and Morimoto, 2004)	AM446
C. elegans: strain AGD3126: zcIs13[hsp-6p::GFP]	(Frankino et al., 2022)	AGD3126
C. elegans: strain AGD3111: dvIs19[pAG15(gst-4p::GFP::NLS)] III; sek-1(km4) X	(Frankino et al., 2022)	AGD3111
C. elegans: strain AGD3013: uth93 ;*amdh-1*(uth29)III; dvIs19[pAG15(gst-4p::GFP::NLS)]; uthEx967[haly-1p::haly-1::haly-1 3' UTR, myo-3p::mCherry]	(Frankino et al., 2022)	AGD3013
C. elegans: strain AGD2530: uth93 ;*amdh-1*(uth29)III; dvIs19[pAG15(gst-4p::GFP::NLS)]	(Frankino et al., 2022)	AGD2530
C. elegans: strain AGD2529: uth92 ;*amdh-1*(uth29)III; dvIs19[pAG15(gst-4p::GFP::NLS)]	(Frankino et al., 2022)	AGD2529
C. elegans: strain AGD2432: pmk-1(km25) IV; dvIs19[pAF15(gst-4p::GFP::NLS)]	(Frankino et al., 2022)	AGD2432
C. elegans: strain AGD2307:amdh-1(uth29)III; dvIs19[pAG15(gst-4p::GFP::NLS)]	(Frankino et al., 2022)	AGD2307
C. elegans: strain AGD2306: amdh-1(uth29)III; rmIs223[pC12C8.1::GFP; rol-6(su1006) II]	(Frankino et al., 2022)	AGD2306
C. *elegans*: strain AGD2053: *zcls4[hsp-4p::GFP]V* (SJ4005 5x backcross)	(Frankino et al., 2022)	AGD2053
C. elegans: strain AGD1848: amdh-1(uth29)III	(Frankino et al., 2022)	AGD1848

C. elegans maintenance

All *C. elegans* strains were maintained at 15°C on NGM plates with OP50 *E. coli* B strain. All experiments were performed at 20°C on RNAi plates (NGM agar, 1 mM IPTG, 100 µg/mL carbenicillin) with HT115 *E. coli* K12 strain bacteria containing the RNAi plasmid pL4440 empty vector as a negative control (EV) or containing sequence to synthesize a double-stranded RNA against a target gene unless otherwise stated. All RNAi constructs were isolated from the Vidal or Ahringer RNAi library and sequence verified before using. For all experiments, eggs were obtained using a standard bleaching protocol (1.8% sodium hypochlorite and 0.375 M KOH) and arrested at the L1 stage overnight in M9 (22 mM KH_2PO_4 monobasic, 42.3 mM Na_2HPO_4, 85.6mM NaCl, 1 mM $MgSO_4$) without food for synchronization. The next day, synchronized L1 animals were placed on HT115 bacteria and grown until day 1 of adulthood. For histidine supplementation experiments, plates were supplemented with 10mM histidine that was buffered with HCl to pH 7.0. Animals were grown on histidine supplemented plates after L1 synchronization for the duration of the entire experiment.

haly-1 rescue experiments were performed using a ~4.3kb amplicon from the genomic DNA of N2 (bristol) animals to include a putative promoter region (~1.1 kb) and complete CDS (~2.6kb, including introns) flanked on each side by the endogenous 5' and 3' UTRs as annotated by wormbase (~0.3kb each). This amplicon was generated in a standard PCR reaction using N2 genomic DNA with the forward primer oPF388 (5' - ttgtccaataaacctttgtcc - 3') and reverse primer oPF389 (5' -tccatataaccctgtaactcc - 3') and sequenced verified using standard Sanger sequencing after PCR purification. Array positive animals were generated by injecting *haly-1(uth92)* or *haly-1(uth93)* animals with purified amplicon at 40 ng/µL along with a co-injection marker (myo-3p::mCherry) at 5 ng/µL. Two independent arrays were isolated from different parent animals for each *haly-1* mutant allele.

Lifespan and Stress Assays

Lifespan measurements were assessed on RNAi plates (standard NGM agar supplemented with 1mM IPTG and 100ug/mL carbenicillin) with HT115 bacteria carrying pL4440 empty vector RNAi. Worms were synchronized by standard bleaching/L1 arresting as described and kept at 20°C throughout the duration of the experiment. Adult worms were moved away from progeny onto fresh plates for the first 5-7 days until progeny were no longer visible and scored every 1 to 2 days until all animals were scored. Animals with bagging, vulval explosions, or other age-unrelated deaths were censored and removed from quantification. For tunicamycin survival assays, animals were moved onto tunicamycin (25 ng/µl) or 1% DMSO plates at D1 of adulthood and scored as described for standard lifespan measurements. For thermotolerance, worms were synchronized by bleaching as described above, L1 arrested, and plated on RNAi plates with HT115 bacteria carrying pL4440 empty vector or other RNAi. At D1, 15-20 worms per plate with 3-4 plates per condition were exposed to 34ºC heat via incubator for 14-15 hours. Plates were then removed from the incubator and manually assessed for movement and pharyngeal pumping, using light head taps where necessary, to determine survival. Worms that displayed internal hatching (bagging) or crawled onto the side of the plate and desiccated were censored and omitted from the final analysis. Percent alive was calculated using the number of living worms divided by the total number of worms excluding censored animals for each strain. For

oxidative stress survival, worms were bleach synchronized, L1 arrested, and plated on RNAi plates with HT115 bacteria carrying empty vector or *daf-2* RNAi. At D1, ~100 animals per condition were transferred to 4-5 NGM plates containing 7.5mM t-booh (Luperox TBH70X, Sigma). Worms were scored for survival every 2 hours, starting at 12 hours, until the 16 hour time point.

Fluorescence imaging and quantification

Image acquisition was performed as previously described (Bar-Ziv et al., 2020). Briefly, day 1 animals were picked under a standard dissection microscope onto a solid NGM plate that contained a ~15µL drop of 100 nM sodium azide. Immobilized worms were aligned head to tail and images were captured on an Echo Revolve R4 microscope equipped with an Olympus 4x Plan Fluorite NA 0.13 objective lens, a standard Olympus FITC filter (ex 470/40; em 525/50; DM 560), and an iPad Pro for the camera and to drive the ECHO software.

To quantify fluorescence, a COPAS large particle biosorter was used as previously described (Bar-Ziv et al., 2020). Data were collected gating for size (time of flight [TOF] and extinction) to exclude eggs and most L1 animals. Data were processed by censoring events that reached the maximum peak height for Green or Extinction measurements (PH Green, PH Ext = 65532) and censoring events < 300 TOF to exclude any remaining L1 animals. For the reporters with low basal fluorescence (AGD2053, AGD3126), data > 0 were included. For reporter strains with visible basal fluorescence (CL2166, AGD2307), data >= 10 were included for subsequent statistical analysis. All fluorescence data were normalized to TOF to account for worm size. For all *amdh-1(uth29)* mutant experiments, 'SKN-1 activation' was quantified by normalizing Green/TOF value for each mutant to the median of the wild type population for each condition. For the MAPK mutant experiments (Figure 2a), 'SKN-1 activation' was quantified by normalizing the Green/TOF value for each mutant fed *amdh-1* RNAi to the median of that mutant fed EV RNAi. All data is plotted as log(FC) SKN-1 activation.

RNA isolation, sequencing and analysis

Animals were bleach synchronized and grown to Day 1 adulthood on empty vector RNAi plates. At least 2,000 animals per condition per replicate were washed off plates using M9 and collected. After a 30 second spin down at 1,000 RCF, M9 was aspirated, replaced with 1mL Trizol, and the tube was immediately frozen in liquid nitrogen to be stored at -80°C for downstream processing. RNA was harvested after 3 freeze thaw cycles in liquid nitrogen/37°C water bath. After the final thaw, 200µL of chloroform were added to the sample, vortexed, and the aqueous phase was collected after centrifugation in a gel phase lock tube. RNA was isolated from the obtained aqueous phase using a Qiagen RNeasy MiniKit according to manufacturer's directions. Library preparation was performed using Kapa Biosystems mRNA Hyper Prep Kit (Roche, product number KK8581) using dual index adapters (KAPA, product number KK8722). Sequencing was performed using Illumina HS4000, mode SR100, through the Vincent J. Coates Genomic Sequencing Core at University of California, Berkeley.

For RNA-seq analysis of *amdh-1(uth29)* mutants, the raw sequencing data were uploaded to the Galaxy project web platform and the public server at usegalaxy.org was used to analyze the data

(Afgan et al., 2016). Paired end reads were aligned using the Kallisto quant tool (Version 0.46.0) with WBcel235 as the reference genome. Fold changes and statistics were generated using the DESeq2 tool with Kallisto quant count files as the input. Volcano plots were generated using the GraphPad Prism version 8.0.0 for Windows (GraphPad Software, San Diego, California USA, www.graphpad.com) on the fold change and adjusted-p values generated by the DESeq2 analysis. For analysis of previously published data, raw reads were downloaded from the Gene Expression Omnibus (GEO), (Accession: GSE123531 and GSE63075) and analyzed as described above. Raw reads for N2 and *amdh-1(uth29)* animals can be accessed on the short read archive (SRA), Bioproject Number PRJNA801069.

EMS mutagenesis screen to find suppressors of SKN-1 activation

amdh-1(uth29); gst-4p::GFP::NLS (strain AGD2307) were mutagenized to find suppressors of *gst-4p::GFP* signal. Briefly, ~150 L4 animals were picked into a 1.5mL eppendorf tube containing 1mL M9 buffer and spun down at 1,000 RPM for 1 minute. The M9 was aspirated from the tube and replaced with 1mL fresh M9 and spun again. To the washed worm pellet, 5µL of EMS (Sigma, M0880-5G) was added, the tube was parafilmed and left nutating at 20C for 4 hours. After incubation, the worms were spun down and rinsed 4 times with 1mL M9. Waste was collected and neutralized with 1:1 KOH before discarding. Rinsed, mutagenized, worms were plated overnight. The next day, mutagenized worms were picked onto 10 large plates seeded with OP50 bacteria, 10 per plate, and allowed to lay eggs for 24 hours. Three days later, adult F1 animals were bleached and plated onto fresh large plates. F2 mutants were screened for suppression of *gst-4p::GFP* under a fluorescent microscope compared to age matched, un-mutagenized, control animals.

Genomic DNA was extracted from mutants of interest using the Puregene Cell and Tissue Kit (Qiagen), as previously described (Lehrbach et al., 2017). 2ug of purified DNA was sheared using a Covaris S220 focused-ultrasonicator to produce ~400 bp fragments. Library preparation was performed with 1ug of sheared DNA using Kapa Biosystems Hyper Prep Kit (Roche, product number KK8504) dual index adapters (KAPA, product number KK8727). Sequencing was performed using the Illumina NovaSeq6000 platform through the Vincent J. Coates Genomic Sequencing Core at University of California, Berkeley. Raw reads were uploaded to the Galaxy project web platform and the public server at usegalaxy.org was used to analyze the data (Afgan et al., 2016). Reads were aligned using the Bowtie2 tool with WBcel235/ce11 as the reference genome. The MiModD tool suite (Baumeister lab) was used on the Variant Allele Contrast (VAC) mapping mode to call, extract and filter variants to compare mutants to the parental, un-mutagenized strain. Causative genes were identified through a combination of genetic complementation, deep sequencing and RNAi phenocopy experiments.

RNAi sub-library construction and screening

Sequence verified sub libraries for chromatin and phosphatase genes were already present in the Dillin lab. To construct kinase, MAPK and TCA cycle sublibraries, clones were streaked out from the vidal and ahringer libraries on LB plates with carbenicillin. Single colonies were picked and grown in LB with carbenicillin and tetracycline, mini prepped and sequenced verified using the M13F primer (below).

M13F: 5’ - GTAAAACGACGGCCAGT - 3’

Clones with clean sequencing results were kept and consolidated into the sequence verified libraries, in 96-well plate format. Genes were identified as kinases, MAPK related or TCA cycle genes using a mixture of literature searching and GO term analysis. Clones that had a correct sequence but one that did not match the listed gene from the vidal and ahringer libraries were still included in the final libraries.

All libraries were screened at least twice on *gst-4p::GFP* reporter animals in an *amdh-1* mutant background, with the exception of the chromatin gene library. The TCA cycle and phosphatase libraries were also screened on *gst-4p::GFP* animals in a wild-type background (basal rep). “Hits” from the screen were defined as RNAi clones that suppressed *amdh-1* mediated SKN-1 activation in both replicates, besides the chromatin hits, where there was only 1 replicate performed. RNAi knockdowns that led to suppression in one replicate of the TCA, MAPK, phosphatase or kinase libraries, or that had opposite direction of effect across replicates, were excluded from further analysis.

Analysis of genes via pathway analysis and STRING

RNAi hits from our screens, as defined above, were entered into WormEnrichr as an unranked list (https://maayanlab.cloud/WormEnrichr/)(Kuleshov et al., 2016). The Kegg 2019 output (under the “pathways” tab) was downloaded and log transformed and plotted. STRING analysis was performed by entering the RNAi hits into the STRING database website, with default settings applied (https://string-db.org/). Predicted interactions were found by increasing the nodes of the network one time on the interface shown on the website (“+ More”).

Contributions of Dillin lab members

Most of the work contained in chapters 1-3 would not have been possible without the contributions of specific Dillin lab members: Talha Siddiqi (TFS), Theo Bolas (TB), Raz Bar-Ziv (RBZ), Holly Gildea (HKG), Hanlin Zhang (HZ) and Ryo Higuchi-Sanabria (RHS). RHS executed early experiments and intellectually contributed to project design/execution. TFS and TB executed stress response reporter experiments and TFS help significantly with design and execution of experiments shown in chapter 4. RBZ assisted with RNA-sequencing analysis. HKG and HZ assisted with early experiments crucial to the direction of the project. All authors assisted with the editing of the manuscript and have provided their consent to use this co-authored work which was released on the pre-print server BioRxiv in February 2022 (Frankino et al., 2022).

Chapter 6: References

(1) Afgan, E., Baker, D., van den Beek, M., Blankenberg, D., Bouvier, D., Čech, M., Chilton, J., Clements, D., Coraor, N., Eberhard, C., et al. (2016). The Galaxy platform for accessible, reproducible and collaborative biomedical analyses: 2016 update. Nucleic Acids Res *44*, W3–W10. https://doi.org/10.1093/nar/gkw343.

(2) Akram, M. (2014). Citric Acid Cycle and Role of its Intermediates in Metabolism. Cell Biochem Biophys *68*, 475–478. https://doi.org/10.1007/s12013-013-9750-1.

(3) Bar-Ziv, R., Frakes, A.E., Higuchi-Sanabria, R., Bolas, T., Frankino, P.A., Gildea, H.K., Metcalf, M.G., and Dillin, A. (2020). Measurements of Physiological Stress Responses in C. Elegans. JoVE (Journal of Visualized Experiments) e61001. https://doi.org/10.3791/61001.

(4) Bender, R.A. (2012). Regulation of the histidine utilization (hut) system in bacteria. Microbiol. Mol. Biol. Rev. *76*, 565–584. https://doi.org/10.1128/MMBR.00014-12.

(5) Bennett, C.F., Vander Wende, H., Simko, M., Klum, S., Barfield, S., Choi, H., Pineda, V.V., and Kaeberlein, M. (2014). Activation of the mitochondrial unfolded protein response does not predict longevity in Caenorhabditis elegans. Nat Commun *5*, 3483. https://doi.org/10.1038/ncomms4483.

(6) Blackwell, T.K., Steinbaugh, M.J., Hourihan, J.M., Ewald, C.Y., and Isik, M. (2015). SKN-1/Nrf, stress responses, and aging in Caenorhabditis elegans. Free Radic Biol Med *88*, 290–301. https://doi.org/10.1016/j.freeradbiomed.2015.06.008.

(7) Bowerman, B., Eaton, B.A., and Priess, J.R. (1992). skn-1, a maternally expressed gene required to specify the fate of ventral blastomeres in the early C. elegans embryo. Cell *68*, 1061–1075. https://doi.org/10.1016/0092-8674(92)90078-Q.

(8) Bowser Revel, H.R., and Magasanik, B. (1958). The Enzymatic Degradation of Urocanic Acid. Journal of Biological Chemistry *233*, 930–935. https://doi.org/10.1016/S0021-9258(18)64681-2.

(9) Boylan, S.A., and Bender, R.A. (1984). Genetic and physical maps of Klebsiella aerogenes genes for histidine utilization (hut). Molec. Gen. Genet. *193*, 99–103. https://doi.org/10.1007/BF00327421.

(10) Calvo, A.C., Pey, A.L., Ying, M., Loer, C.M., and Martinez, A. (2008). Anabolic function of phenylalanine hydroxylase in Caenorhabditis elegans. The FASEB Journal *22*, 3046–3058. https://doi.org/10.1096/fj.08-108522.

(11) Chen, E.Y., Tan, C.M., Kou, Y., Duan, Q., Wang, Z., Meirelles, G.V., Clark, N.R., and Ma'ayan, A. (2013). Enrichr: interactive and collaborative HTML5 gene list enrichment analysis tool. BMC Bioinformatics *14*, 128. https://doi.org/10.1186/1471-2105-14-128.

(12) Choe, K.P., Przybysz, A.J., and Strange, K. (2009). The WD40 Repeat Protein WDR-23 Functions with the CUL4/DDB1 Ubiquitin Ligase To Regulate Nuclear Abundance and Activity of SKN-1 in Caenorhabditis elegans. Mol Cell Biol *29*, 2704–2715. https://doi.org/10.1128/MCB.01811-08.

(13) Chong, S., Dugast-Darzacq, C., Liu, Z., Dong, P., Dailey, G.M., Cattoglio, C., Heckert, A., Banala, S., Lavis, L., Darzacq, X., et al. (2018). Imaging dynamic and selective low-

complexity domain interactions that control gene transcription. Science eaar2555. https://doi.org/10.1126/science.aar2555.

(14) Crombie, T.A., Tang, L., Choe, K.P., and Julian, D. (2016). Inhibition of the oxidative stress response by heat stress in Caenorhabditis elegans. Journal of Experimental Biology jeb.135327. https://doi.org/10.1242/jeb.135327.

(15) DeBerardinis, R.J., and Thompson, C.B. (2012). Cellular metabolism and disease: what do metabolic outliers teach us? Cell *148*, 1132–1144. https://doi.org/10.1016/j.cell.2012.02.032.

(16) Deng, J., Dai, Y., Tang, H., and Pang, S. (2020). SKN-1 Is a Negative Regulator of DAF-16 and Somatic Stress Resistance in Caenorhabditis elegans. G3: Genes, Genomes, Genetics *10*, 1707–1712. https://doi.org/10.1534/g3.120.401203.

(17) Edwards, C., Canfield, J., Copes, N., Brito, A., Rehan, M., Lipps, D., Brunquell, J., Westerheide, S.D., and Bradshaw, P.C. (2015). Mechanisms of amino acid-mediated lifespan extension in Caenorhabditis elegans. BMC Genetics *16*, 8. https://doi.org/10.1186/s12863-015-0167-2.

(18) Efeyan, A., Comb, W.C., and Sabatini, D.M. (2015). Nutrient Sensing Mechanisms and Pathways. Nature *517*, 302–310. https://doi.org/10.1038/nature14190.

(19) Ferguson, A.A., Springer, M.G., and Fisher, A.L. (2010). skn-1-Dependent and -Independent Regulation of aip-1 Expression following Metabolic Stress in Caenorhabditis elegans. Molecular and Cellular Biology https://doi.org/10.1128/MCB.01340-09.

(20) Fisher, A.L., Page, K.E., Lithgow, G.J., and Nash, L. (2008). The Caenorhabditis elegans K10C2.4 Gene Encodes a Member of the Fumarylacetoacetate Hydrolase Family. J Biol Chem *283*, 9127–9135. https://doi.org/10.1074/jbc.M708341200.

(21) Frankino, P.A., Siddiqi, T.F., Bolas, T., Bar-Ziv, R., Gildea, H.K., Zhang, H., Higuchi-Sanabria, R., and Dillin, A. (2022). SKN-1 is a metabolic surveillance factor that monitors amino acid catabolism to control stress resistance. 2022.02.03.479044. https://doi.org/10.1101/2022.02.03.479044.

(22) Ganner, A., Gerber, J., Ziegler, A.-K., Li, Y., Kandzia, J., Matulenski, T., Kreis, S., Breves, G., Klein, M., Walz, G., et al. (2019). CBP-1/p300 acetyltransferase regulates SKN-1/Nrf cellular levels, nuclear localization, and activity in C. elegans. Experimental Gerontology *126*, 110690. https://doi.org/10.1016/j.exger.2019.110690.

(23) Glover-Cutter, K.M., Lin, S., and Blackwell, T.K. (2013). Integration of the Unfolded Protein and Oxidative Stress Responses through SKN-1/Nrf. PLoS Genet *9*, e1003701. https://doi.org/10.1371/journal.pgen.1003701.

(24) Goh, G.Y.S., Martelli, K.L., Parhar, K.S., Kwong, A.W.L., Wong, M.A., Mah, A., Hou, N.S., and Taubert, S. (2014). The conserved Mediator subunit MDT-15 is required for oxidative stress responses in Caenorhabditis elegans. Aging Cell *13*, 70–79. https://doi.org/10.1111/acel.12154.

(25) Goh, G.Y.S., Winter, J.J., Bhanshali, F., Doering, K.R.S., Lai, R., Lee, K., Veal, E.A., and Taubert, S. (2018). NHR-49/HNF4 integrates regulation of fatty acid metabolism with a protective transcriptional response to oxidative stress and fasting. Aging Cell *17*, e12743. https://doi.org/10.1111/acel.12743.

(26) Grushko, D., Boocholez, H., Levine, A., and Cohen, E. (2021). Temporal requirements of SKN-1/NRF as a regulator of lifespan and proteostasis in Caenorhabditis elegans. PLOS ONE *16*, e0243522. https://doi.org/10.1371/journal.pone.0243522.

(27) van der Hoeven, R., McCallum, K.C., Cruz, M.R., and Garsin, D.A. (2011). Ce-Duox1/BLI-3 Generated Reactive Oxygen Species Trigger Protective SKN-1 Activity via p38 MAPK Signaling during Infection in C. elegans. PLoS Pathog *7*, e1002453. https://doi.org/10.1371/journal.ppat.1002453.

(28) Holeček, M. (2020). Histidine in Health and Disease: Metabolism, Physiological Importance, and Use as a Supplement. Nutrients *12*, 848. https://doi.org/10.3390/nu12030848.

(29) Hu, Q., D'Amora, D.R., MacNeil, L.T., Walhout, A.J.M., and Kubiseski, T.J. (2017). The Oxidative Stress Response in Caenorhabditis elegans Requires the GATA Transcription Factor ELT-3 and SKN-1/Nrf2. Genetics *206*, 1909–1922. https://doi.org/10.1534/genetics.116.198788.

(30) Inoue, H., Hisamoto, N., An, J.H., Oliveira, R.P., Nishida, E., Blackwell, T.K., and Matsumoto, K. (2005). The C. elegans p38 MAPK pathway regulates nuclear localization of the transcription factor SKN-1 in oxidative stress response. Genes Dev *19*, 2278–2283. https://doi.org/10.1101/gad.1324805.

(31) Jones, P., Patel, K., and Rakheja, D. (2020). Chapter 23 - Disorder: Tyrosinemia type 1. In A Quick Guide to Metabolic Disease Testing Interpretation (Second Edition), P. Jones, K. Patel, and D. Rakheja, eds. (Academic Press), pp. 121–125.

(32) Kanarek, N., Keys, H.R., Cantor, J.R., Lewis, C.A., Chan, S.H., Kunchok, T., Abu-Remaileh, M., Freinkman, E., Schweitzer, L.D., and Sabatini, D.M. (2018). Histidine catabolism is a major determinant of methotrexate sensitivity. Nature *559*, 632–636. https://doi.org/10.1038/s41586-018-0316-7.

(33) Kanehisa, M., Sato, Y., Kawashima, M., Furumichi, M., and Tanabe, M. (2016). KEGG as a reference resource for gene and protein annotation. Nucleic Acids Research *44*, D457–D462. https://doi.org/10.1093/nar/gkv1070.

(34) Kell, A., Ventura, N., Kahn, N., and Johnson, T.E. (2007). Activation of SKN-1 by novel kinases in Caenorhabditis elegans. Free Radic Biol Med *43*, 1560–1566. https://doi.org/10.1016/j.freeradbiomed.2007.08.025.

(35) Kim, D.H., Liberati, N.T., Mizuno, T., Inoue, H., Hisamoto, N., Matsumoto, K., and Ausubel, F.M. (2004). Integration of Caenorhabditis elegans MAPK pathways mediating immunity and stress resistance by MEK-1 MAPK kinase and VHP-1 MAPK phosphatase. Proceedings of the National Academy of Sciences *101*, 10990–10994. https://doi.org/10.1073/pnas.0403546101.

(36) Kuleshov, M.V., Jones, M.R., Rouillard, A.D., Fernandez, N.F., Duan, Q., Wang, Z., Koplev, S., Jenkins, S.L., Jagodnik, K.M., Lachmann, A., et al. (2016). Enrichr: a comprehensive gene set enrichment analysis web server 2016 update. Nucleic Acids Res *44*, W90-97. https://doi.org/10.1093/nar/gkw377.

(37) Lehrbach, N.J., Ji, F., and Sadreyev, R. (2017). Next-Generation Sequencing for Identification of EMS-Induced Mutations in Caenorhabditis elegans. Curr Protoc Mol Biol *117*, 7.29.1-7.29.12. https://doi.org/10.1002/cpmb.27.

(38) Li, T.Y., Sleiman, M.B., Li, H., Gao, A.W., Mottis, A., Bachmann, A.M., El Alam, G., Li, X., Goeminne, L.J.E., Schoonjans, K., et al. (2021). The transcriptional coactivator CBP/p300 is an evolutionarily conserved node that promotes longevity in response to mitochondrial stress. Nat Aging *1*, 165–178. https://doi.org/10.1038/s43587-020-00025-z.

(39) Link, C.D., and Johnson, C.J. (2002). [42] - Reporter Transgenes for Study of Oxidant Stress in Caenorhabditis elegans. In Methods in Enzymology, C.K. Sen, and L. Packer, eds. (Academic Press), pp. 497–505.

(40) Lo, J.Y., Spatola, B.N., and Curran, S.P. (2017). WDR23 regulates NRF2 independently of KEAP1. PLoS Genet *13*, e1006762. https://doi.org/10.1371/journal.pgen.1006762.

(41) Ma, Q. (2013). Role of Nrf2 in Oxidative Stress and Toxicity. Annu Rev Pharmacol Toxicol *53*, 401–426. https://doi.org/10.1146/annurev-pharmtox-011112-140320.

(42) Martínez-Reyes, I., and Chandel, N.S. (2020). Mitochondrial TCA cycle metabolites control physiology and disease. Nat Commun *11*, 102. https://doi.org/10.1038/s41467-019-13668-3.

(43) McGaha, T.L., Huang, L., Lemos, H., Metz, R., Mautino, M., Prendergast, G.C., and Mellor, A.L. (2012). Amino acid catabolism: a pivotal regulator of innate and adaptive immunity. Immunol Rev *249*, 135–157. https://doi.org/10.1111/j.1600-065X.2012.01149.x.

(44) Merkwirth, C., Jovaisaite, V., Durieux, J., Matilainen, O., Jordan, S.D., Quiros, P.M., Steffen, K.K., Williams, E.G., Mouchiroud, L., Tronnes, S.U., et al. (2016). Two Conserved Histone Demethylases Regulate Mitochondrial Stress-Induced Longevity. Cell *165*, 1209–1223. https://doi.org/10.1016/j.cell.2016.04.012.

(45) Molinaro, A., Bel Lassen, P., Henricsson, M., Wu, H., Adriouch, S., Belda, E., Chakaroun, R., Nielsen, T., Bergh, P.-O., Rouault, C., et al. (2020). Imidazole propionate is increased in diabetes and associated with dietary patterns and altered microbial ecology. Nat Commun *11*, 5881. https://doi.org/10.1038/s41467-020-19589-w.

(46) Morley, J.F., and Morimoto, R.I. (2004). Regulation of Longevity in Caenorhabditis elegans by Heat Shock Factor and Molecular Chaperones. Mol. Biol. Cell *15*, 657–664. https://doi.org/10.1091/mbc.E03-07-0532.

(47) Morrow, G., and Tanguay, R.M. (2017). Biochemical and Clinical Aspects of Hereditary Tyrosinemia Type 1. In Hereditary Tyrosinemia: Pathogenesis, Screening and Management, R.M. Tanguay, ed. (Cham: Springer International Publishing), pp. 9–21.

(48) Nhan, J.D., Turner, C.D., Anderson, S.M., Yen, C.-A., Dalton, H.M., Cheesman, H.K., Ruter, D.L., Uma Naresh, N., Haynes, C.M., Soukas, A.A., et al. (2019). Redirection of SKN-1 abates the negative metabolic outcomes of a perceived pathogen infection. Proc Natl Acad Sci U S A *116*, 22322–22330. https://doi.org/10.1073/pnas.1909666116.

(49) Niwa, T., Katsuzaki, T., Miyazaki, S., Miyazaki, T., Ishizaki, Y., Hayase, F., Tatemichi, N., and Takei, Y. (1997). Immunohistochemical detection of imidazolone, a novel advanced glycation end product, in kidneys and aortas of diabetic patients. J Clin Invest *99*, 1272–1280. .

(50) Nolfi-Donegan, D., Braganza, A., and Shiva, S. (2020). Mitochondrial electron transport chain: Oxidative phosphorylation, oxidant production, and methods of measurement. Redox Biol *37*, 101674. https://doi.org/10.1016/j.redox.2020.101674.

(51) Oliveira, R.P., Abate, J.P., Dilks, K., Landis, J., Ashraf, J., Murphy, C.T., and Blackwell, T.K. (2009). Condition-adapted stress and longevity gene regulation by Caenorhabditis elegans SKN-1/Nrf. Aging Cell *8*, 524–541. https://doi.org/10.1111/j.1474-9726.2009.00501.x.

(52) Omar, A.M., Abdelghany, T.M., Abdel-Bakky, M.S., Alahdal, A.M., Radwan, M.F., and El-Araby, M.E. (2018). Design, Synthesis and Antiproliferative Activities of Oxidative Stress Inducers Based on 2-Styryl-3,5-dihydro-4*H*-imidazol-4-one Scaffold. Chemical and Pharmaceutical Bulletin *66*, 967–975. https://doi.org/10.1248/cpb.c18-00398.

(53) Paek, J., Lo, J.Y., Narasimhan, S.D., Nguyen, T.N., Glover-Cutter, K., Robida-Stubbs, S., Suzuki, T., Yamamoto, M., Blackwell, T.K., and Curran, S.P. (2012). Mitochondrial SKN-1/Nrf Mediates a Conserved Starvation Response. Cell Metab *16*, 526–537. https://doi.org/10.1016/j.cmet.2012.09.007.

(54) Pakos-Zebrucka, K., Koryga, I., Mnich, K., Ljujic, M., Samali, A., and Gorman, A.M. (2016). The integrated stress response. EMBO Rep *17*, 1374–1395. https://doi.org/10.15252/embr.201642195.

(55) Pang, S., Lynn, D.A., Lo, J.Y., Paek, J., and Curran, S.P. (2014). SKN-1 and Nrf2 couples proline catabolism with lipid metabolism during nutrient deprivation. Nat Commun *5*, 1–8. https://doi.org/10.1038/ncomms6048.

(56) Papp, D., Csermely, P., and Sőti, C. (2012). A Role for SKN-1/Nrf in Pathogen Resistance and Immunosenescence in Caenorhabditis elegans. PLOS Pathogens *8*, e1002673. https://doi.org/10.1371/journal.ppat.1002673.

(57) Rao, D.R., and Greenberg, D.M. (1961). Studies on the Enzymic Decomposition of Urocanic Acid: IV. PURIFICATION AND PROPERTIES OF 4(5)-IMIDAZOLONE-5(4)-PROPIONIC ACID HYDROLASE. Journal of Biological Chemistry *236*, 1758–1763. https://doi.org/10.1016/S0021-9258(19)63297-7.

(58) Ravichandran, M., Priebe, S., Grigolon, G., Rozanov, L., Groth, M., Laube, B., Guthke, R., Platzer, M., Zarse, K., and Ristow, M. (2018). Impairing L-Threonine Catabolism Promotes Healthspan through Methylglyoxal-Mediated Proteohormesis. Cell Metabolism *27*, 914-925.e5. https://doi.org/10.1016/j.cmet.2018.02.004.

(59) Romero, R., Sánchez-Rivera, F.J., Westcott, P.M.K., Mercer, K.L., Bhutkar, A., Muir, A., González Robles, T.J., Lamboy Rodríguez, S., Liao, L.Z., Ng, S.R., et al. (2020). Keap1 mutation renders lung adenocarcinomas dependent on Slc33a1. Nat Cancer *1*, 589–602. https://doi.org/10.1038/s43018-020-0071-1.

(60) Sekhar, K.R., Rachakonda, G., and Freeman, M.L. (2010). Cysteine-based regulation of the CUL3 adaptor protein Keap1. Toxicol Appl Pharmacol *244*, 21–26. https://doi.org/10.1016/j.taap.2009.06.016.

(61) Shao, J., He, K., Wang, H., Ho, W.S., Ren, X., An, X., Wong, M.K., Yan, B., Xie, D., Stamatoyannopoulos, J., et al. (2013). Collaborative Regulation of Development but Independent Control of Metabolism by Two Epidermis-specific Transcription Factors in Caenorhabditis elegans*. Journal of Biological Chemistry *288*, 33411–33426. https://doi.org/10.1074/jbc.M113.487975.

(62) Smith, K.T., and Workman, J.L. (2012). Chromatin Proteins: Key Responders to Stress. PLoS Biol *10*, e1001371. https://doi.org/10.1371/journal.pbio.1001371.

(63) Steinbaugh, M.J., Narasimhan, S.D., Robida-Stubbs, S., Moronetti Mazzeo, L.E., Dreyfuss, J.M., Hourihan, J.M., Raghavan, P., Operaña, T.N., Esmaillie, R., and Blackwell, T.K. (2015). Lipid-mediated regulation of SKN-1/Nrf in response to germ cell absence. ELife *4*, e07836. https://doi.org/10.7554/eLife.07836.

(64) Sykiotis, G.P., and Bohmann, D. (2010). Stress-Activated Cap'n'collar Transcription Factors in Aging and Human Disease. Sci Signal *3*, re3. https://doi.org/10.1126/scisignal.3112re3.

(65) Szklarczyk, D., Gable, A.L., Nastou, K.C., Lyon, D., Kirsch, R., Pyysalo, S., Doncheva, N.T., Legeay, M., Fang, T., Bork, P., et al. (2021). The STRING database in 2021: customizable protein-protein networks, and functional characterization of user-uploaded gene/measurement sets. Nucleic Acids Res *49*, D605–D612. https://doi.org/10.1093/nar/gkaa1074.

(66) Tabachnick, J. (1957). Urocanic acid, the major acid-soluble, ultraviolet-absorbing compound in guinea pig epidermis. Archives of Biochemistry and Biophysics *70*, 295–298. https://doi.org/10.1016/0003-9861(57)90107-8.

(67) Tang, H., and Pang, S. (2016). Proline Catabolism Modulates Innate Immunity in Caenorhabditis elegans. Cell Reports *17*, 2837–2844. https://doi.org/10.1016/j.celrep.2016.11.038.

(68) Tang, L., and Choe, K.P. (2015). Characterization of skn-1/wdr-23 phenotypes in Caenorhabditis elegans; pleiotrophy, aging, glutathione, and interactions with other longevity pathways. Mechanisms of Ageing and Development *149*, 88–98. https://doi.org/10.1016/j.mad.2015.06.001.

(69) Tian, Y., Garcia, G., Bian, Q., Steffen, K.K., Joe, L., Wolff, S., Meyer, B.J., and Dillin, A. (2016). Mitochondrial Stress Induces Chromatin Reorganization to Promote Longevity and UPR(mt). Cell *165*, 1197–1208. https://doi.org/10.1016/j.cell.2016.04.011.

(70) Tullet, J.M.A., Hertweck, M., Hyung An, J., Baker, J., Hwang, J.Y., Liu, S., Oliveira, R.P., Baumeister, R., and Blackwell, T.K. (2008). Direct inhibition of the longevity promoting factor SKN-1 by Insulin-like signaling in C. elegans. Cell *132*, 1025–1038. https://doi.org/10.1016/j.cell.2008.01.030.

(71) Tullet, J.M.A., Green, J.W., Au, C., Benedetto, A., Thompson, M.A., Clark, E., Gilliat, A.F., Young, A., Schmeisser, K., and Gems, D. (2017). The SKN-1/Nrf2 transcription factor can protect against oxidative stress and increase lifespan in C. elegans by distinct mechanisms. Aging Cell *16*, 1191–1194. https://doi.org/10.1111/acel.12627.

(72) Wang, J., Robida-Stubbs, S., Tullet, J.M.A., Rual, J.-F., Vidal, M., and Blackwell, T.K. (2010). RNAi Screening Implicates a SKN-1–Dependent Transcriptional Response in Stress Resistance and Longevity Deriving from Translation Inhibition. PLOS Genetics *6*, e1001048. https://doi.org/10.1371/journal.pgen.1001048.

(73) Wu, C.-W., Deonarine, A., Przybysz, A., Strange, K., and Choe, K.P. (2016). The Skp1 Homologs SKR-1/2 Are Required for the Caenorhabditis elegans SKN-1 Antioxidant/Detoxification Response Independently of p38 MAPK. PLoS Genet *12*, e1006361. https://doi.org/10.1371/journal.pgen.1006361.

(74) Ženíšek, A., Král, J.A., and Hais, I.M. (1955). "Sun-screening" effect of urocanic acid. Biochimica et Biophysica Acta *18*, 589–591. https://doi.org/10.1016/0006-3002(55)90167-0.

(75) Zhang, S., Xu, C., Larrimore, K.E., and Ng, D.T.W. (2017). Slp1-Emp65: A Guardian Factor that Protects Folding Polypeptides from Promiscuous Degradation. Cell *171*, 346-357.e12. https://doi.org/10.1016/j.cell.2017.08.036.

(76) Zhou, J., Wang, X., Wang, M., Chang, Y., Zhang, F., Ban, Z., Tang, R., Gan, Q., Wu, S., Guo, Y., et al. (2018). The lysine catabolite saccharopine impairs development by disrupting mitochondrial homeostasis. Journal of Cell Biology *218*, 580–597. https://doi.org/10.1083/jcb.201807204.

Chapter 7: Appendix

Table 1: RNAi Screen Results for Amino Acid Catabolism Genes

Gene	Score	Source
ahcy-1	-3	Ahringer Library
ahcy-1	-3	Vidal Library
gta-1	-1	Ahringer Library
let-504	0	Ahringer Library
gcsh-2	0	Ahringer Library
bckd-1B	0	Ahringer Library
glna-3	0	Ahringer Library
alh-6	0	Ahringer Library
T01H3.3	0	Ahringer Library
K01C8.1	0	Ahringer Library
gstk-1	0	Ahringer Library
alh-8	0	Ahringer Library
glna-1	0	Ahringer Library
uroc-1	0	Ahringer Library
T25B9.1	0	Ahringer Library
afmd-1	0	Ahringer Library
C15B12.8	0	Ahringer Library
tdo-2	0	Ahringer Library
acdh-6	0	Ahringer Library
Y39A1A.3/epg-6	0	Ahringer Library
bckd-1A	0	Ahringer Library
bckd-1A	0	Ahringer Library
qdpr-1	0	Ahringer Library
ZK180.5	0	Ahringer Library
srbc-64	0	Ahringer Library
R102.4	0	Ahringer Library
prdh-1	0	Ahringer Library
Y7A9A.1	0	Ahringer Library
Y79H2A.12/lin-40	0	Ahringer Library

T19H12.6	0	Ahringer Library
C31H2.4	0	Ahringer Library
T21F4.1/T22B7.8	0	Ahringer Library
C15B12.1	0	Ahringer Library
got-2.2	0	Ahringer Library
gcsh-1	0	Ahringer Library
cblc-1	0	Ahringer Library
ethe-1	0	Vidal Library
T03D8.6	0	Vidal Library
gcsh-1	0	Vidal Library
B0250.5	0	Vidal Library
gst-42	0	Vidal Library
haly-1	0	Vidal Library
T25B9.1	0	Vidal Library
afmd-1	0	Vidal Library
qdpr-1	0	Vidal Library
got-2.2	0	Vidal Library
glna-3	0	Vidal Library
B0250.5	0	Vidal Library
gcst-1	0	Vidal Library
oatr-1	0	Vidal Library
K01C8.1	0	Vidal Library
acdh-6	0	Vidal Library
Y53G8B.1	0	Vidal Library
hpd-1	0	Vidal Library
afmd-2	0	Vidal Library
gcsh-2	0	Vidal Library
gst-43	0	Vidal Library
got-2.1	0	Vidal Library
C53D5.5	0	Vidal Library
gstk-1	0	Vidal Library
F30A10.9/stn-1	1	Ahringer Library

gldc-1	1	Ahringer Library
gsr-1	1	Ahringer Library
H14N18.4	1	Vidal Library
Y97E10A2.2	1	Vidal Library
uroc-1	1	Vidal Library
hach-1	1	Vidal Library
M04B2.4	1	Vidal Library
amdh-1	1	Vidal Library
hach-1	2	Ahringer Library
T07E3.3	2	Ahringer Library
hgo-1	2	Vidal Library
pah-1	2	Vidal Library
gcs-1	3	Ahringer Library
gss-1	3	Ahringer Library
fah-1	3	Ahringer Library
fah-1	3	Vidal Library
gcs-1	3	Vidal Library
H14N18.4	not scored	Ahringer Library
haao-1	not scored	Ahringer Library
E01A2.1	not scored	Vidal Library
Y45G12C.1	not scored	Vidal Library

Table 2: RNAi Screen Results for TCA Cycle Genes

Gene	Library	amdh-1(uth29) rep 1	amdh-1(uth29) rep 2	Basal rep 1
dlst-1	Ahringer	-2	-3	-1
ogdh-1	Ahringer	-2	-3	-2
dlst-1	Vidal	-2	-2	-1
fum-1	Ahringer	-1	0	0
mev-1	Ahringer	-1	0	0
sdhb-1	Ahringer	0	-1	0
aco-1	Ahringer	0	0	0
bckd-1A	Ahringer	0	0	0
bckd-1A	Vidal	0	0	0

bckd-1B	Ahringer	0	0	0
bckd-1B	Vidal	0	0	0
fum-1	Vidal	0	0	0
icl-1	Ahringer	0	0	0
idh-1	Ahringer	0	0	0
idh-2	Ahringer	0	0	0
idh-2	Vidal	0	0	0
idhg-1	Ahringer	0	0	0
idhg-2	Ahringer	0	0	0
mdh-1	Vidal	0	0	0
mdh-1	Ahringer	0	0	0
mev-1	Vidal	0	0	0
ogdh-2	Ahringer	0	0	0
sdha-1	Ahringer	0	0	0
sdha-1	Ahringer	0	0	0
sdha-2	Vidal	0	0	1
sdhb-1	Vidal	0	0	0
sdhd-1	Vidal	0	0	1
suca-1	Ahringer	0	0	0
sucg-1	Vidal	0	0	0
sucl-1	Vidal	0	0	0
sucl-1	Ahringer	0	0	0
ttc-4	Vidal	0	0	1
Y57A10A.29	Vidal	0	0	0
sucl-2	Ahringer	1	-1	1
aco-1	Vidal	1	0	0
idhb-1	Vidal	1	0	0
idhb-1	Ahringer	1	0	0
sucg-1	Ahringer	1	0	0
idha-1	Ahringer	2	0	2
cts-1	Vidal	3	0	3
aco-2	Ahringer	3	1	3

cts-1	Ahringer	3	1	3
gss-1	Ahringer	3	2	3
mdh-2	Vidal	3	2	2
mdh-2	Ahringer	3	2	2

Table 3: RNAi Screen Results for MAPK genes

Gene	Library	amdh-1(uth29) rep 1	amdh-1(uth29) rep 2
vhp-1	Ahringer	-3	-3
vhp-1	Vidal	-3	-3
puf-8	Vidal	1	1 or 2
gck-1	Ahringer	0	-1
gck-2	Ahringer	0	-1
kin-18	Ahringer	0	-1
kin-18	Vidal	0	-1
ndk-1	Ahringer	0	-1
riok-1	Ahringer	0	-1
stam-1	Vidal	0	-1
T22B11.4	Ahringer	0	-1
zak-1	Ahringer	0	-1
kgb-2	Ahringer	0	1
lit-1	Vidal	lethal	0
pat-4	Ahringer	-1/-2	0
ppm-2	Vidal	-1	0
y106G60.4	Ahringer	-1	0
y106G6E.1	Ahringer	-1	0
B0252.1	Vidal	0	0
c49c3.10	Ahringer	0	0
daf-7	Ahringer	0	0
daf-7	Vidal	0	0
dbl-1	Ahringer	0	0
dbl-1	Vidal	0	0
dlk-1	Ahringer	0	0

egrh-1	Ahringer	0	0
ergh-1	Vidal	0	0
f21f3.2	Ahringer	0	0
F21f3.2	Vidal	0	0
fem-3	Vidal	0	0
gck-2	Vidal	0	0
gska-3	Ahringer	0	0
inx-19	Ahringer	0	0
jnk-1	Vidal	0	0
k11h12.9	Ahringer	0	0
kgb-1	Ahringer	0	0
kgb-1	Vidal	0	0
lit-1	Ahringer	0	0
mapk-15	Ahringer	0	0
max-2	Ahringer	0	0
max-2	Vidal	0	0
mek-1	Ahringer	0	0
mek-2	Vidal	0	0
mes-1	Vidal	0	0
mes-1	Ahringer	0	0
mkk-4	Ahringer	0	0
mom-4	Ahringer	0	0
mom-4	Vidal	0	0
mpk-1	Ahringer	0	0
mpk-2	Ahringer	0	0
mpk-2	Vidal	0	0
msp-77	Ahringer	0	0
msp-77	Vidal	0	0
msp-79	Ahringer	0	0
ndk-1	Vidal	0	0
nipi-3	Ahringer	0	0
nsy-1	Ahringer	0	0

oma-1	Ahringer	0	0
oma-2	Ahringer	0	0
pak-1	Ahringer	0	0
pak-1	Vidal	0	0
pak-2	Ahringer	0	0
pmk-1	Ahringer	0	0
pmk-1	Vidal	0	0
pmk-2	Ahringer	0	0
pmk-2	Vidal	0	0
pmk-3	Ahringer	0	0
ppm-1.A	Vidal	0	0
ppm-2	Ahringer	0	0
rpm-1	Ahringer	0	0
sek-4	Vidal	0	0
sek-5	Ahringer	0	0
strd-1	Vidal	0	0
svh-1	Ahringer	0	0
svh-1	Vidal	0	0
svh-2	Ahringer	0	0
T14E8.2	Ahringer	0	0
t22b11.4	Vidal	0	0
tig-2	Vidal	0	0
tir-1	Ahringer	0	0
tir-1	Vidal	0	0
tpa-1	Ahringer	0	0
unc-43	Ahringer	0	0
unc-43	Vidal	0	0
V51B9A.9	Vidal	0	0
y106G6E.1	Vidal	0	0
Y51B9A.9	Ahringer	0	0

Table 4: RNAi Screen Results for Chromatin Genes

Gene	Library	amdh-1(uth29) rep 1	Notes
lin-41	Ahringer	-3	Sick/Bagging
cbp-1	Ahringer	-3	No progeny
lex-1	Ahringer	-2	
his-34	Ahringer	-2	
cec-1	Ahringer	-2	
zfp-1	Ahringer	-1	
sox-2	Ahringer	-1	bagging
lin-61	Ahringer	-1	
lin-40	Ahringer	-1	
his-65	Ahringer	-1	
his-57	Ahringer	-1	
his-43	Ahringer	-1	Heterozygous suppression
W03D8.4	Ahringer	0	
Y105E8C.d	Ahringer	0	
Y48G1A 53.a	Ahringer	0	
H20J04.f	Ahringer	0	
ZK945.5	Ahringer	0	
F26H11.3	Ahringer	0	
Y53F4B.d	Ahringer	0	
Y43F4B.1	Ahringer	0	
Y53G8A 6046.a	Ahringer	0	
Y55B1B 119.b	Ahringer	0	
Y71H2 375.b	Ahringer	0	
Y73B6A.f	Ahringer	0	
Y62E10A.e	Ahringer	0	
Y57G11C.19	Ahringer	0	
Y105C5A.a	Ahringer	0	
Y105C5A.r	Ahringer	0	
Y51H4A.l	Ahringer	0	

Y41D4A 2615.a	Ahringer	0	
D1014.9	Ahringer	0	
T11A5.1	Ahringer	0	
W01C8.2	Ahringer	0	
T01C1.3	Ahringer	0	
C52G5.1	Ahringer	0	
ZK1240.3	Ahringer	0	
ZK1240.2	Ahringer	0	
ZK1240.1	Ahringer	0	
ZC155.2	Ahringer	0	
Y75B8A.6	Ahringer	0	
Y113G7B.14	Ahringer	0	
xnd-1	Ahringer	0	
wapl-1	Ahringer	0	
utx-1	Ahringer	0	
taf-9	Ahringer	0	
taf-4	Ahringer	0	
taf-3	Ahringer	0	
taf-12	Ahringer	0	
taf-11.2	Ahringer	0	
taf-11.1	Ahringer	0	
taf-1	Ahringer	0	
T26A5.8	Ahringer	0	
T24G10.2	Ahringer	0	
T23H2.3	Ahringer	0	
T13F2.2	Ahringer	0	
T10D4.6	Ahringer	0	
T07F8.4	Ahringer	0	
T05A12.4	Ahringer	0	
T01B7.5	Ahringer	0	
swsn-9	Ahringer	0	
swsn-7	Ahringer	0	

swsn-4	Ahringer	0	
spt-4	Ahringer	0	
spr-5	Ahringer	0	
spe-44	Ahringer	0	
sox-3	Ahringer	0	
snpc-4	Ahringer	0	
snfc-5	Ahringer	0	
smrc-1	Ahringer	0	
sir-2.1	Ahringer	0	
sin-3	Ahringer	0	
set-9	Ahringer	0	
set-8	Ahringer	0	
set-6	Ahringer	0	
set-5	Ahringer	0	
set-4	Ahringer	0	
set-30	Ahringer	0	
set-22	Ahringer	0	
set-20	Ahringer	0	
set-2	Ahringer	0	
set-19	Ahringer	0	
set-17	Ahringer	0	
set-16	Ahringer	0	
set-15	Ahringer	0	
set-14	Ahringer	0	
set-12	Ahringer	0	
set-11	Ahringer	0	
set-10	Ahringer	0	
set-1	Ahringer	0	
sepa-1	Ahringer	0	
saeg-2	Ahringer	0	
rbr-2	Ahringer	0	
rad-54.L	Ahringer	0	

rad-54.B	Ahringer	0	
rad-26	Ahringer	0	
psr-1	Ahringer	0	
phf-34	Ahringer	0	
phf-33	Ahringer	0	
phf-32	Ahringer	0	
phf-30	Ahringer	0	
pdcd-2	Ahringer	0	
pbrm-1	Ahringer	0	
ntl-9	Ahringer	0	
nhl-3	Ahringer	0	
nhl-2	Ahringer	0	
nfyc-1	Ahringer	0	
ncl-1	Ahringer	0	
natc-2	Ahringer	0	
mys-2	Ahringer	0	
mys-1	Ahringer	0	
mrg-1	Ahringer	0	
met-2	Ahringer	0	
mes-4	Ahringer	0	
mel-28	Ahringer	0	
madd-2	Ahringer	0	
mab-10	Ahringer	0	
M03C11.8	Ahringer	0	
lin-49	Ahringer	0	
lin-35	Ahringer	0	
let-19	Ahringer	0	
K09A11.1	Ahringer	0	
jmjd-5	Ahringer	0	
jmjd-3.3	Ahringer	0	
jmjd-3.2	Ahringer	0	
jmjd-3.1	Ahringer	0	

jmjd-3.1	Ahringer	0	
jmjd-1.2	Ahringer	0	
jmjd-1.1	Ahringer	0	
isw-1	Ahringer	0	
htz-1	Ahringer	0	
htas-1	Ahringer	0	
hpo-15	Ahringer	0	
hpl-2	Ahringer	0	
hpl-1	Ahringer	0	
hmg-6	Ahringer	0	
hmg-5	Ahringer	0	
hmg-3	Ahringer	0	
hmg-20	Ahringer	0	
hmg-12	Ahringer	0	
hmg-11	Ahringer	0	
hmg-1.2	Ahringer	0	
hmg-1.1	Ahringer	0	
his-74	Ahringer	0	
his-73	Ahringer	0	
his-72	Ahringer	0	
his-70	Ahringer	0	
his-7	Ahringer	0	
his-69	Ahringer	0	
his-68	Ahringer	0	
his-64	Ahringer	0	
his-62	Ahringer	0	
his-61	Ahringer	0	
his-59	Ahringer	0	
his-5	Ahringer	0	
his-47	Ahringer	0	
his-42	Ahringer	0	
his-33	Ahringer	0	

his-3	Ahringer	0	
his-24	Ahringer	0	
his-16	Ahringer	0	
hil-8	Ahringer	0	
hil-5	Ahringer	0	
hil-4	Ahringer	0	
hil-1	Ahringer	0	
heri-1	Ahringer	0	
hda-6	Ahringer	0	
hda-4	Ahringer	0	
hda-3	Ahringer	0	
hda-2	Ahringer	0	
hda-11	Ahringer	0	
hda-10	Ahringer	0	
hda-1	Ahringer	0	Protruding vulva
hcp-3	Ahringer	0	
ham-3	Ahringer	0	
gna-2	Ahringer	0	
gna-1	Ahringer	0	
gmeb-3	Ahringer	0	
gmeb-2	Ahringer	0	
gmeb-1	Ahringer	0	
glo-4	Ahringer	0	
gfl-1	Ahringer	0	
gei-8	Ahringer	0	
F59E12.1	Ahringer	0	
F59A7.8	Ahringer	0	
F55C5.6	Ahringer	0	
F54F2.9	Ahringer	0	
F54E12.2	Ahringer	0	
F47G9.4	Ahringer	0	
F43G9.12	Ahringer	0	

F43G6.4	Ahringer	0	
F36G3.2	Ahringer	0	
F36A2.10	Ahringer	0	
F28F8.7	Ahringer	0	
F22F1.3	Ahringer	0	
F13C5.2	Ahringer	0	
F10E7.11	Ahringer	0	
F07A11.4	Ahringer	0	
egl-9	Ahringer	0	
dro-1	Ahringer	0	
dpff-1	Ahringer	0	
dnj-11	Ahringer	0	
ctbp-1	Ahringer	0	
csb-1	Ahringer	0	
cpar-1	Ahringer	0	
chd-3	Ahringer	0	
chd-1	Ahringer	0	
cfi-1	Ahringer	0	
cec-6	Ahringer	0	
cec-5	Ahringer	0	
cec-3	Ahringer	0	
cdc-6	Ahringer	0	
cdc-14	Ahringer	0	
C56G2.15	Ahringer	0	
C52B9.8	Ahringer	0	
C49F5.5	Ahringer	0	
C34B7.1	Ahringer	0	
C29F9.5	Ahringer	0	
C25F9.5	Ahringer	0	
C16C10.4	Ahringer	0	
C06A5.3	Ahringer	0	
C01B12.8	Ahringer	0	

btf-1	Ahringer	0	
bra-2	Ahringer	0	
bra-1	Ahringer	0	
bed-2	Ahringer	0	
baz-2	Ahringer	0	
B0336.7	Ahringer	0	
B0281.3	Ahringer	0	
B0261.1	Ahringer	0	
B0019.2	Ahringer	0	
attf-6	Ahringer	0	
attf-3	Ahringer	0	
attf-2	Ahringer	0	
athp-3	Ahringer	0	
athp-1	Ahringer	0	
anat-1	Ahringer	0	
amx-3	Ahringer	0	
amx-2	Ahringer	0	
amx-1	Ahringer	0	
ada-2	Ahringer	0	
Y39B6B.u	Ahringer	0	
cdc-5L	Ahringer	0	
T10B5.4	Ahringer	1	
set-18	Ahringer	1	
lin-59	Ahringer	1	
hira-1	Ahringer	1	
top-2	Ahringer	2	Low Fecundity
sir-2.3	Ahringer	2	
sir-2.2	Ahringer	2	
hmg-4	Ahringer	2	Protruding vulva no progeny
his-71	Ahringer	2	
F33H1.4	Ahringer	2	
skp-1	Ahringer	lethal	

C04A2.2	Ahringer	N/A	
Y48G8A 3051.d	Ahringer	N/A	
spt-5	Ahringer	N/A	
sox-4	Ahringer	N/A	
lsd-1	Ahringer	N/A	
his-35	Ahringer	N/A	
hil-3	Ahringer	N/A	
F20D6.9	Ahringer	N/A	
drap-1	Ahringer	N/A	
attf-5	Ahringer	N/A	

Table 5: RNAi Screen Results for Phosphatase Genes

Gene	amdh-1(uth29) rep 1	amdh-1(uth29) rep 2	Basal Rep 1	Notes
vhp-1	-2	-3	-2	Small worms
T16G12.6	-2	-2	-1	
hpo-8	-1	-2	-2	
gfi-2	-1	-1	0	
mel-11	-1	-1	N/A	Sterile
F54C8.4	-1	-1	-1	
tax-6	-1	-1	-2	
F53B2.5	1	-1	-1	
C33F10.8	N/A	-1	0	
cki-2	N/A	-1	0	
B0511.7	0	-1	0	
cki-1	0	-1	0	
F58G1.3	0	-1	-1	
lin-12	0	-1	-1	
inpp-1	0	-1	0	

K07F5.6	-3	0	-1	
F22D6.9	-2	0	0	
pde-12	-1	0	0	
Y5F2A.3	-1	0	0	
ZK809.1	-1	0	0	
ccr-4	-1	0	0	
F49E11.7	-1	0	-1	
ima-1	-1	0	0	
T04F3.3	0	0	0	
R31.2	0	0	0	
F40G12.10	0	0	0	
akt-1	0	0	0	
ppm-1	0	0	0	
pph-1	0	0	0	
pptr-2	0	0	0	
C43E11.5	1	0	0	
ima-2	1	0	0	
F55H12.2	1	0	0	
K09F6.3	1	0	-1	
F25H5.7	1	0	0	
sur-6	1	0	0	
fem-2	1	0	0	
R10F2.6	1	0	0	
phlp-2	1	0	0	
sma-4	1	0	-1	

F20H11.4	1	0	0	
M04G7.2	1	0	0	
T16G12.7	1	0	0	
R01H10.7	1	0	0	
CC8.c	1	0	0	
B0478.2	1	0	-1	
C24D10.1	1	0	0	
C34D4.2	1	0	0	
C33H5.16	1	0	0	
xpo-3	1	0	0	
F36H1.3	1	0	0	
C47A4.3	1	0	0	
F20D6.6	1	0	0	
F25B3.4	1	0	0	
C06G1.5	1	0	0	
sma-2	N/A	0	0	
pho-5	N/A	0	N/A	
ZK757.2	N/A	0	0	
C42C1.2	N/A	0		
soc-1	N/A	0	0	
C53D5.b	0	0	0	
nab-1	0	0	0	
gsp-3	0	0	0	
W03F11.4	0	0	-1	
W03D8.2	0	0	0	

F40E3.5	0	0	0	
gsp-4	0	0	0	
F47B3.7	0	0	-1	
egg-4	0	0	0	
F47B3.2	0	0	0	
egg-5	0	0	0	
mtm-1	0	0	0	
T28F4.3	0	0	0	
F26A3.4	0	0	0	
T22C1.8	0	0	0	
F55F8.7	0	0	0	
ZK484.7	0	0	0	
T27A3.5	0	0	0	
ppfr-2	0	0	0	
H06O01.4	0	0	0	
M05B5.1	0	0	0	
hpo-7	0	0	N/A	
ppfr-1	0	0	0	
C04F12.8	0	0	-1	
rsa-1	0	0	0	
Y18H1A_68.a	0	0	0	
dep-1	0	0	0	
pir-1	0	0	0	
ptp-2	0	0	0	
sma-6	0	0	0	

M05D6.3	0	0	0	
F28C6.8	0	0	0	
C18E9.7	0	0	0	
ZK938.1	0	0	0	
pef-1	0	0	0	
F52H3.6	0	0	0	
ZK945.8	0	0	0	
C07E3.4	0	0	-1	
C06A1.3	0	0	0	
egg-3	0	0	0	
R03D7.8	0	0	0	
plpr-1	0	0	0	
VW02B12L.2	0	0	-1	
R06B10.1	0	0	0	
ppm-2	0	0	0	
szy-2	0	0	0	
R06B10.2	0	0	0	
R155.3	0	0	0	
T20B6.1	0	0	0	
H06I04.5	0	0	-1	
pph-6	0	0	0	
R10E4.9	0	0	0	
ida-1	0	0	0	
C30A5.4	0	0	0	
C16A3.2	0	0	0	

sma-3	0	0	0	
kap-1	0	0	0	
upp-1	0	0	0	
F44B9.9	0	0	0	
Y119D3_464.f	0	0	0	
daf-18	0	0	0	
K03H1.8	0	0	0	
W09D10.4	0	0	0	
F54F12.1	0	0	0	
ZC477.2	0	0	0	
ZC477.3	0	0	0	
F36H12.10	0	0	0	
ZK354.8	0	0	0	
C17H12.3	0	0	0	
C17H12.5	0	0	0	
lip-1	0	0	0	
K07F5.8	0	0	0	
ima-3	0	0	-1	sterile
C46A5.1	0	0	0	
C33H5.8	0	0	0	
F57H12.5	0	0	0	
F42G8.8	0	0	0	
C27B7.6	0	0	-1	
ptp-4	0	0	0	
F38H4.4	0	0	0	

C24F3.2	0	0	-1	
R09E10.2	0	0	0	
Y69E1A.4	0	0	0	
F14F9.5	0	0	0	
Y62E10A.m	0	0	0	
Y116A8C.37	0	0	0	
Y41D4A_3192.b	0	0	0	
Y69A2A_2991.c	0	0	0	
F23B12.1	0	0	0	
Y40H4A.2	0	0	0	
Y80D3B.f	0	0	0	
Y39B6B.e	0	0	0	
Y39B6B.ff	0	0	0	
F48F5.1	0	0	0	
H02F09.4	0	0	0	
F38E9.3	0	0	0	
T19D2.2	-1	1	0	
R08C7.8	1	1	0	
ZK354.9	1	1	0	
F08F3.5	1	1	0	
H18N23.a	0	1	0	
let-92	-3	N/A	N/A	Lethal
paa-1	-1	N/A	N/A	Lethal
xpo-2	1	N/A	-1	Sterile
W01B6.6	N/A	N/A	N/A	

dbl-1	N/A	N/A	0	
C09H5.7	1		0	

Table 6: RNAi Screen Results for Kinase Genes

Gene	Library	amdh-1(uth29) rep 1	amdh-1(uth29) rep 2	Notes
kin-19	Vidal	-3	-3	
nekl-2	Vidal	-1	-3	
alh-13	Vidal	-1	-1	
ppk-1	Ahringer	-2	-1	
pkc-3	Vidal	-1	-2	
pat-4	Ahringer	-1	-1	
let-754	Ahringer	-2	-2	
kin-2	Ahringer	-3	-3	Lethal
lit-1	Vidal	0	-3	
let-754	Vidal	0	-3	
m7.7	Vidal	-3	1	
clpf-1	Vidal	0	-2	
sgk-1	Ahringer	-2	0	
C34F11.5	Ahringer	-2	0	
mop-25.3	Vidal	-1	0	
Y50D4B.6	Vidal	-1	0	
Y38H8A.3/C39H7.1	Vidal	-1	0	
pyk-2	Vidal	-1	0	
ver-3	Vidal	-1	0	
kin-3	Vidal	0	-1	
aakb-2	Vidal	0	-1	
cyb-2.1	Vidal	0	-1	
cks-1	Vidal	0	-1	
rei-1	Vidal	0	-1	
Y39E4B.6	Vidal	0	-1	
kin-1	Vidal	0	-1	
pstk-1	Vidal	0	-1	

D2045.5	Vidal	0	-1	
E02C12.8	Vidal	0	-1	
kin-10	Vidal	0	-1	
hxk-1	Vidal	0	-1	
gcn-1	Vidal	0	-1	
F23E4.5	Vidal	0	-1	
mek-2	Vidal	0	-1	
aakg-1	Vidal	0	-1	
hpk-1	Ahringer	-1	0	
gska-3	Ahringer	-1	0	
daf-1	Ahringer	-1	0	
ver-3	Ahringer	0	-1	
F22F1.2	Ahringer	0	-1	
cki-1	Vidal	0	0	
F40F8.1	Vidal	0	0	
pmk-1	Vidal	0	0	
Y22D7AR.6	Vidal	0	0	
aakb-1	Vidal	0	0	
twf-2	Vidal	0	0	
cyb-1	Vidal	0	0	
ckk-1	Vidal	0	0	
F47F2.1	Vidal	0	0	
prk-1	Vidal	0	0	
sma-6	Vidal	0	0	
plk-3	Vidal	0	0	
unc-43	Vidal	0	0	
jnk-1	Vidal	0	0	
mom-4	Vidal	0	0	
cye-1	Vidal	0	0	
kin-15	Vidal	0	0	
ppk-2	Vidal	0	0	
argk-1	Vidal	0	0	

F33B2.4	Vidal	0	0	
F28C10.3	Vidal	0	0	
guk-1	Vidal	0	0	
mbk-2	Vidal	0	0	
ZK1127.4	Vidal	0	0	
ZC434.8	Vidal	0	0	
EO2H4.6	Vidal	0	0	
F52B5.2	Vidal	0	0	
elpc-4	Vidal	0	0	
EO2H1.6	Vidal	0	0	
KO4CL5	Vidal	0	0	
Y17G7B.10	Vidal	0	0	
akt-1	Vidal	0	0	
T22B11.4	Vidal	0	0	
pyk-1	Vidal	0	0	
lin-18	Vidal	0	0	
akt-2	Vidal	0	0	
strd-1	Vidal	0	0	
ZK354.2	Vidal	0	0	
F21F3.2	Vidal	0	0	
pgk-1	Vidal	0	0	
EO2D9.1	Vidal	0	0	
cyd-1	Vidal	0	0	
Y77E11A.2	Vidal	0	0	
sad-1	Vidal	0	0	
taf-1	Vidal	0	0	
aak-2	Vidal	0	0	
cit-1.1	Vidal	0	0	
F30A10.3	Vidal	0	0	
dgk-3	Vidal	0	0	
C56G2.5	Vidal	0	0	
F37A4.2	Vidal	0	0	

Y69F12A.1	Vidal	0	0	
cdka-1	Vidal	0	0	
wee-1.3	Vidal	0	0	
pck-2	Vidal	0	0	
T21G5.1	Vidal	0	0	
hxk-2	Vidal	0	0	
aap-1	Vidal	0	0	
cerk-1	Vidal	0	0	
toe-4	Vidal	0	0	
Y47GCA.13	Vidal	0	0	
kin-14	Vidal	0	0	
Y106G6A.1	Vidal	0	0	
ndk-1	Vidal	0	0	
nekl-3	Vidal	0	0	
pfkb-1.1	Vidal	0	0	
ire-1	Vidal	0	0	
cdk-12	Vidal	0	0	
chk-2/T08D2.7	Vidal	0	0	
cyb-1/cyb-2.1/2.2	Vidal	0	0	
bub-1	Vidal	0	0	
cdk-5	Vidal	0	0	
gcy-15	Vidal	0	0	
gcy-21	Vidal	0	0	
kin-16	Vidal	0	0	
ZC581.9	Vidal	0	0	
ver-1	Vidal	0	0	
R02F2.1	Vidal	0	0	
zyg-8	Vidal	0	0	
pdxk-1	Vidal	0	0	
F26E4.5	Vidal	0	0	
R06A10.4	Vidal	0	0	
C34B2.3	Vidal	0	0	

F23C8.8	Vidal	0	0	
F10G8.2	Vidal	0	0	
C47B2.2	Vidal	0	0	
comp-1 NO MATCH	Vidal	0	0	
F33D11.7/C34B2.12	Vidal	0	0	
rsks-1	Vidal	0	0	
M03C11.1	Vidal	0	0	
pck-1	Vidal	0	0	
frk-1	Vidal	0	0	
kin-26	Vidal	0	0	
ttbk-4	Vidal	0	0	
F34H12.9/R13H9.6	Vidal	0	0	
C55C3.4	Vidal	0	0	
F11E6.8	Vidal	0	0	
ZK596.2	Vidal	0	0	
gcy-8	Vidal	0	0	
F32B6.4	Vidal	0	0	
B0001.4	Vidal	0	0	
R11E3.1	Vidal	0	0	
nol-9	Vidal	0	0	
dkf-1	Vidal	0	0	
dapk-1	Vidal	0	0	
F54H5.2	Vidal	0	0	
M05D6.1/F35C11.3	Vidal	0	0	
tbck-1	Vidal	0	0	
Y106G6E.1	Vidal	0	0	
prpf-4	Vidal	0	0	
pps-1	Vidal	0	0	
K09B11.5	Vidal	0	0	
F14H3.12	Vidal	0	0	
C50H2.7	Vidal	0	0	
E02C12.12	Vidal	0	0	

egl-4	Vidal	0	0	
Y43C5B.2	Vidal	0	0	
dyf-18	Vidal	0	0	
D2024.1	Vidal	0	0	
lin-2	Vidal	0	0	
E02C12.11	Vidal	0	0	
C25A8.5	Vidal	0	0	
Y116A8C.24	Vidal	0	0	
C05C12.1	Vidal	0	0	
H06H21.8	Vidal	0	0	
Y11D7A.8	Vidal	0	0	
Y105C5A.24	Vidal	0	0	
prk-2	Vidal	0	0	
sel-5	Vidal	0	0	
wee-1.1	Vidal	0	0	
Y53F4B.1	Vidal	0	0	
mtk-1	Vidal	0	0	
cya-2	Vidal	0	0	
T19D12.5	Vidal	0	0	
W07G4.3	Vidal	0	0	
T25B9.4	Vidal	0	0	
gcy-5	Vidal	0	0	
kin-18	Vidal	0	0	
sorf-1	Vidal	0	0	
T06C10.3	Vidal	0	0	
slc-25A18.2	Vidal	0	0	
nhr-291	Ahringer	0	0	
gcy-20	Ahringer	0	0	
TO8D2.7	Ahringer	0	0	
par-4	Ahringer	0	0	
R0C2.6	Ahringer	0	0	
prde-1	Ahringer	0	0	

F36H9.1	Ahringer	0	0	
gcy-9	Ahringer	0	0	
sid-3	Ahringer	0	0	
mick-1	Ahringer	0	0	
C36B7.2	Ahringer	0	0	
dlg-1	Ahringer	0	0	
F16B12.7	Ahringer	0	0	
F39Fl0.2	Ahringer	0	0	
pix-1	Ahringer	0	0	
svh-2	Ahringer	0	0	
T14E8.2	Ahringer	0	0	
mek-1	Ahringer	0	0	
C55B6.5	Ahringer	0	0	
R04A9.7	Ahringer	0	0	
rei-2	Ahringer	0	0	
T07D1.3	Ahringer	0	0	
aakg-4	Ahringer	0	0	
kin-29	Ahringer	0	0	
dtmk-1	Ahringer	0	0	
C04F6.7	Ahringer	0	0	
cst-1	Ahringer	0	0	
dtmk-1	Ahringer	0	0	
ddr-1	Ahringer	0	0	
sek-5	Ahringer	0	0	
magi-1	Ahringer	0	0	
gcy-18	Ahringer	0	0	
Y38H8A.4	Ahringer	0	0	
ced-3	Ahringer	0	0	
ksr-1	Ahringer	0	0	
F08F1.9	Ahringer	0	0	
trk-1	Ahringer	0	0	
mkk-4	Ahringer	0	0	

mig-15	Ahringer	0	0	
cdk-11.2	Ahringer	0	0	
ver-4	Ahringer	0	0	
trk-1	Ahringer	0	0	
K08H2.5	Ahringer	0	0	
odr-1	Ahringer	0	0	
irk-3	Ahringer	0	0	
nipi-3	Ahringer	0	0	
aakg-2	Ahringer	0	0	
dtmk-1	Ahringer	0	0	
Zk666.8	Ahringer	0	0	
ZK673.2	Ahringer	0	0	
R09D1.13	Ahringer	0	0	
D1044.1	Ahringer	0	0	
Y48B6A.10	Ahringer	0	0	
C26E6.1	Ahringer	0	0	
C26E6.1	Ahringer	0	0	
ver-3	Ahringer	0	0	
abl-1	Ahringer	0	0	
F09A5.2	Ahringer	0	0	
piki-1	Ahringer	0	0	
pnk-4	Ahringer	0	0	
hex-1	Ahringer	0	0	
lurp-2	Ahringer	0	0	
mes-1	Ahringer	0	0	
gcy-11	Ahringer	0	0	
pifk-1	Ahringer	0	0	
C29F7.2	Ahringer	0	0	
C01C4.3	Ahringer	0	0	
F09A5.2	Ahringer	0	0	
F46H5.3	Ahringer	0	0	
T07F12.4	Ahringer	0	0	

C55B6.1	Ahringer	0	0	
C29F7.3	Ahringer	0	0	
gakh-1	Ahringer	0	0	
srv-5	Ahringer	0	0	
ZC373.3	Ahringer	0	0	
Y12A6A.1	Ahringer	0	0	
T25D5.4/wts-1	Ahringer	0	0	
gcy-14	Ahringer	0	0	
dkf-2	Ahringer	0	0	
F38E1.3	Ahringer	0	0	
C56A3.8	Ahringer	0	0	
tag-191	Ahringer	0	0	
lurp-3	Ahringer	0	0	
c38c3.4	Ahringer	0	0	
T16G1.3	Ahringer	0	0	
K09C6.2/C28A5.6	Ahringer	0	0	
cdkl-1	Ahringer	0	0	
ZC123.4	Ahringer	0	0	
F23C8.7	Ahringer	0	0	
riok-1	Ahringer	0	0	
unc-89	Ahringer	0	0	
W03G9.5	Ahringer	0	0	
gcy-28	Ahringer	0	0	
lfe-2	Ahringer	0	0	
F59A3.8	Ahringer	0	0	
hil-8	Ahringer	0	0	
san-1	Ahringer	0	0	
comp-1	Ahringer	0	0	
pnk-1	Ahringer	0	0	
hasp-1	Ahringer	0	0	
rskn-2	Ahringer	0	0	
cdc-48.3	Ahringer	0	0	

H05L14.1	Ahringer	0	0	
cdk-8	Ahringer	0	0	
wts-1	Ahringer	0	0	
Y106G6D.4	Ahringer	0	0	
C35E7.10	Ahringer	0	0	
lrk-1	Ahringer	0	0	
src-2	Ahringer	0	0	
R11F4.1	Ahringer	0	0	
F53C3.1	Ahringer	0	0	
F59A6.4	Ahringer	0	0	
F11G11.13	Ahringer	0	0	
ZK177.2	Ahringer	0	0	
F59E12.3	Ahringer	0	0	
mps-1	Ahringer	0	0	
cki-2	Ahringer	0	0	
cdk-11.1	Ahringer	0	0	
T05C12.1	Ahringer	0	0	
sphk-1	Ahringer	0	0	
cam-1	Ahringer	0	0	
mop-25.2	Ahringer	0	0	
old-1	Ahringer	0	0	
R05H5.4	Ahringer	0	0	
mnk-1	Ahringer	0	0	
C14A4.13	Ahringer	0	0	
lurp-1	Ahringer	0	0	
R03D7.5	Ahringer	0	0	
W02B12.12	Ahringer	0	0	
vps-15	Ahringer	0	0	
max-2	Ahringer	0	0	
gcn-2	Ahringer	0	0	
grk-2	Ahringer	0	0	
ver-2	Ahringer	0	0	

W04B5.5	Ahringer	0	0	
cic-1	Ahringer	0	0	
ckb-2	Ahringer	0	0	
F26A1.4	Ahringer	0	0	
F25F2.1	Ahringer	0	0	
F26A1.3	Ahringer	0	0	
C28A5.6	Ahringer	0	0	
coq-8	Ahringer	0	0	
skpt-1	Ahringer	0	0	
mapk-15	Ahringer	0	0	
efk-1	Ahringer	0	0	
F57B9.8	Ahringer	0	0	
F31E3.2	Ahringer	0	0	
atg-13	Ahringer	0	0	
cit-1.2	Ahringer	0	0	
kin-31	Ahringer	0	0	
ZK507.3	Ahringer	0	0	
riok-3	Ahringer	0	0	
cya-1	Ahringer	0	0	
W06F12.3	Ahringer	0	0	
tpa-1	Ahringer	0	0	
kgb-1	Ahringer	0	0	
gtf-2H1	Ahringer	0	0	
pig-1	Ahringer	0	0	
K11H12.9	Ahringer	0	0	
mak-2	Ahringer	0	0	
cmk-1	Ahringer	0	0	
W03F8.2	Ahringer	0	0	
C39H7.1	Ahringer	0	0	
ttbk-2	Ahringer	0	0	
T11F8.4	Ahringer	0	0	
F36H12.9	Ahringer	0	0	

pct-1	Ahringer	0	0	
F21D5.5	Ahringer	0	0	
F08B4.3	Ahringer	0	0	
C49E8.1	Ahringer	0	0	
wnk-1	Ahringer	0	0	
F49C12.7	Ahringer	0	0	
kin-21	Ahringer	0	0	
kin-24	Ahringer	0	0	
KO9E4.1	Vidal	1	0	
toe-2	Vidal	1	0	
cdk-7	Vidal	0	1	
chk-1	Vidal	0	1	
pdhk-2	Vidal	0	1	
riok-3	Vidal	0	1	
pmk-2	Vidal	0	1	
kin-5	Vidal	0	1	
Y73F8A.24	Vidal	0	1	
cka-1	Vidal	0	1	
ZK354.6	Vidal	0	1	
B0257.1	Vidal	0	1	
R10H10.6	Vidal	0	1	
dtmk-1	Vidal	0	1	
CCnk-1	Ahringer	0	1	
cdk-9	Ahringer	0	1	
dlk-1	Ahringer	0	1	
ckb-1	Ahringer	0	1	
plk-1	Vidal	1	1	
vrk-1	Vidal	0	2	
unc-51	Vidal	0	2	
cdc-48.3	Vidal	0	2	
C17C3.11	Vidal	0	2	
cdk-1	Vidal	2	2	

F19B6.1	Vidal	2	3	
egl-15	Ahringer	-1	N/A	Bagging